

NASA TECHNICAL NOTE



NASA TN D-7001

C.1

NASA TN D-7001

LOAN COPY: RETURN
AFWL (DOGL)
KIRTLAND AFB, N.



ANNULAR SLIT COLLOID THRUSTER RESEARCH AND DEVELOPMENT

by Kenneth W. Stark and William A. Burton

*Goddard Space Flight Center
Greenbelt, Md. 20771*

NATIONAL AERONAUTICS AND SPACE ADMINISTRATION • WASHINGTON, D. C.





0133699

1. Report No. NASA TN D-7001	2. Government Accession No.		3. Recipient's Catalog No.	
4. Title and Subtitle Annular Slit Colloid Thruster Research and Development		5. Report Date May 1971		
		6. Performing Organization Code		
7. Author(s) Kenneth W. Stark and William A. Burton		8. Performing Organization Report No. G-1002		
9. Performing Organization Name and Address Goddard Space Flight Center Greenbelt, Maryland 20771		10. Work Unit No.		
		11. Contract or Grant No.		
12. Sponsoring Agency Name and Address National Aeronautics and Space Administration Washington, D.C. 20546		13. Type of Report and Period Covered Technical Note		
		14. Sponsoring Agency Code		
15. Supplementary Notes				
16. Abstract This report is a continuation of the annular slit colloid thruster development described in NASA TN D-5305. Numerous tests were conducted with thrusters having nominal diameters of 0.080 in. and 0.76 in. During this program the phenomenon of glow spray was encountered. Reduced flow rates and various propellant combinations were tested as possible ways to eliminate glow spray. Based on the results of this program, the use of sodium iodide and 1,2,6-hexanetriol as a propellant offers significant advantages over the use of sodium iodide and glycerol. An improvement in performance was noted with both propellants when flow rates were reduced; however, over extended periods of operation, there are indications that electron back bombardment degrades performance. An important factor in the success of the colloid R&D program is the reduction or elimination of the effects of electron back bombardment.				
17. Key Words Suggested by Author Colloid Thrusters Annular Thrusters Propellant Solutions Glow Spray		18. Distribution Statement Unclassified—Unlimited		
19. Security Classif. (of this report) Unclassified	20. Security Classif. (of this page) Unclassified	21. No. of Pages 56	22. Price * \$3.00	

CONTENTS

	Page
LIST OF SYMBOLS	v
INTRODUCTION	1
ANNULAR THRUSTER DESIGN THEORY	1
DATA REDUCTION	3
LABORATORY APPARATUS AND TEST PROCEDURE	9
Horizontal Firing	9
Vertical Firing Downward	10
Vertical Firing Upward	11
Time of Flight Techniques	11
RESEARCH PROGRAM AND RESULTS	14
Thruster Performance Testing	23
Thruster Geometry Variations	31
Propellant Investigation	35
Flow Control Tests	49
CONCLUSIONS	55
ACKNOWLEDGMENTS	56
References	56

LIST OF SYMBOLS

ACMR	=	average charge to mass ratio
d	=	time of flight (TOF) distance
g_0	=	acceleration of gravity
h	=	$R_2 - R_1$
I_c	=	collector current
I_{ext}	=	extractor current
I_0	=	TOF collector current at time = 0
I_s	=	slit source current
I_{scr}	=	screen current
I_{sp}	=	specific impulse
i	=	current
l	=	length of annulus
\dot{m}_c	=	mass flow as measured at the collector
\dot{m}_t	=	total mass flow rate, $(I_s/I_c)\dot{m}_c$
P	=	pressure differential across the annulus
P_f	=	feed pressure
P_t	=	thruster power
Q	=	volume flow rate
q/m	=	square mean root (SMR) charge to mass ratio
R_1	=	inner radius
R_2	=	outer radius
T_c	=	thrust as measured at the collector
T_t	=	total thrust, $(I_s/I_c)T_c$
t_f	=	TOF time at current = 0
V_{ext}	=	extractor voltage
V_s	=	slit source voltage
v	=	velocity
η_b	=	beam efficiency
μ	=	viscosity
ρ	=	density

ANNULAR SLIT COLLOID THRUSTER RESEARCH AND DEVELOPMENT

by

Kenneth W. Stark

and

William A. Burton

Goddard Space Flight Center

INTRODUCTION

The development and operational feasibility of the higher thrust annular slit colloid thruster has been previously reported (References 1 and 2). Research in the optimization of performance and further study of the performance characteristics associated with this new geometry were the next tasks to be undertaken.

During this research, it was observed that good performance was normally accompanied by a visible glow emanating from the annulus. This behavior has been termed "glow spray". Because the cause and effect relationship of the glow spray were unknown, it was decided to try to obtain the required performance in the absence of glow spray.

It was reasoned that the glow intensity was dependent upon the propellant vapor background in the vacuum chamber; therefore, new propellant solutions with vapor pressures lower than that of the standard NaI-glycerol solution were sought. Also, reduced propellant flow rates were employed.

ANNULAR THRUSTER DESIGN THEORY

The exact equation for flow through a concentric annulus (Reference 3) (Figure 1) is

$$Q = \frac{\pi P}{8\mu l} (R_2^2 - R_1^2) \left[R_2^2 + R_1^2 - \frac{R_2^2 - R_1^2}{\ln R_2/R_1} \right]. \quad (1)$$

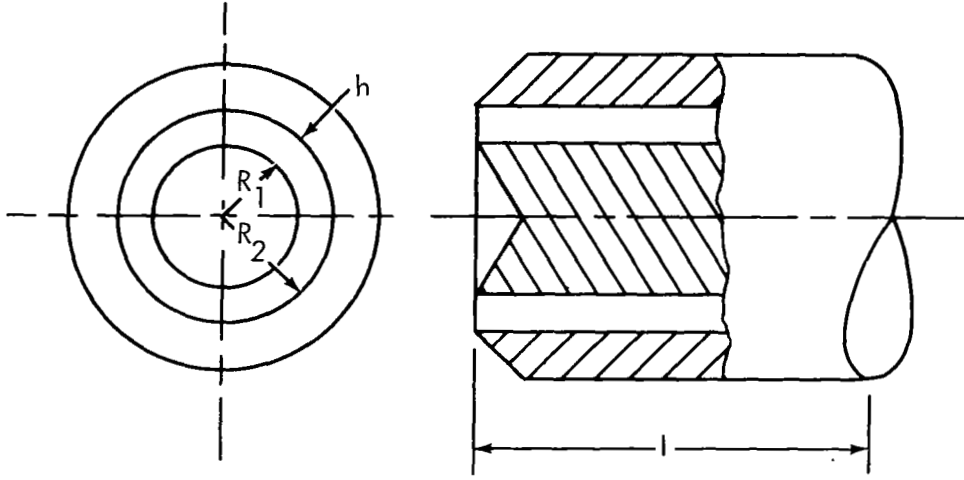


Figure 1-Concentric annulus diagram.

However, this equation is awkward to use for thruster design since normally the desired flow rate Q is known and the annular gap $R_2 - R_1$ and radius R_1 are the terms to be determined.

As an alternative, the simplified and more practical expression (Reference 4)

$$Q = \frac{\Delta P \pi R_1 h^3}{6 \mu l} \quad (2)$$

is used.

It can be shown that if a series expansion is substituted for $\ln R_2/R_1$ in Equation 1 and h is set equal to $R_2 - R_1$ in Equation 2, the two equations are equal when R_2 approaches R_1 .

Figure 2 is a series of parametric curves relating mass flow rate to the ratio R/l . In this case the annulus serves as the flow-controlling orifice; however, as described later in the report, flow rates were required that were much lower than would be practical to control through an annulus. In some cases, therefore, it is necessary to use a flow control orifice upstream rather than depend on the annulus for flow control. The annulus gap still remains critical at the rims because spraying occurs there and one of the critical factors in performance is to minimize the residence time of the propellant surface exposed to the vacuum. The reasons for this will be explained later in this report.

Figure 3 is a graph of I_{sp} versus source voltage at various q/m 's. Figure 3 is an idealized relationship showing the particular minimum voltage necessary to obtain a given q/m and I_{sp} . In reality, performance also depends upon thruster geometry, material erosion, propellant properties such as conductivity, vapor pressure, viscosity, and surface tension, and extractor configuration and voltage. As yet it has been impossible to relate these various parameters either theoretically or empirically in a reliable and meaningful equation. To date then, the most practical way of designing a colloid thruster is to use the data available from existing tests and the basic flow equations. This results in a hybrid thruster in which all previous data were used as design guides, which makes it possible to pursue further testing in the continual refining process of colloid thruster evolution.

Table 1 lists the original design parameters for both the small and large annular thrusters obtained from Equation 2. Figures 4 and 5 are photographs of the large and small annular thrusters, respectively. Table 2 lists the original performance goals for both thrusters.

DATA REDUCTION

Ideally, the optimum procedure for testing and evaluating thruster performance would be to use a direct thrust measurement system and an absolute flow measuring device. Unfortunately, at this time, suitable means for direct measurement of thrust and flow rates for these experimental laboratory models are not available.

Present methods of reducing data use a technique developed early in the history of colloid thruster technology (References 5 and 6). Basically, this method employs the time of flight (TOF) trace, which is numerically integrated to yield thrust, specific impulse, charge-to-mass ratios, efficiency, mass flow rates, and average particle velocity.

A TOF trace is obtained by the simultaneous grounding of the thruster voltage and the recording of the collector current decay curve caused by the particles in flight after grounding. A typical TOF curve is shown in Figure 6.

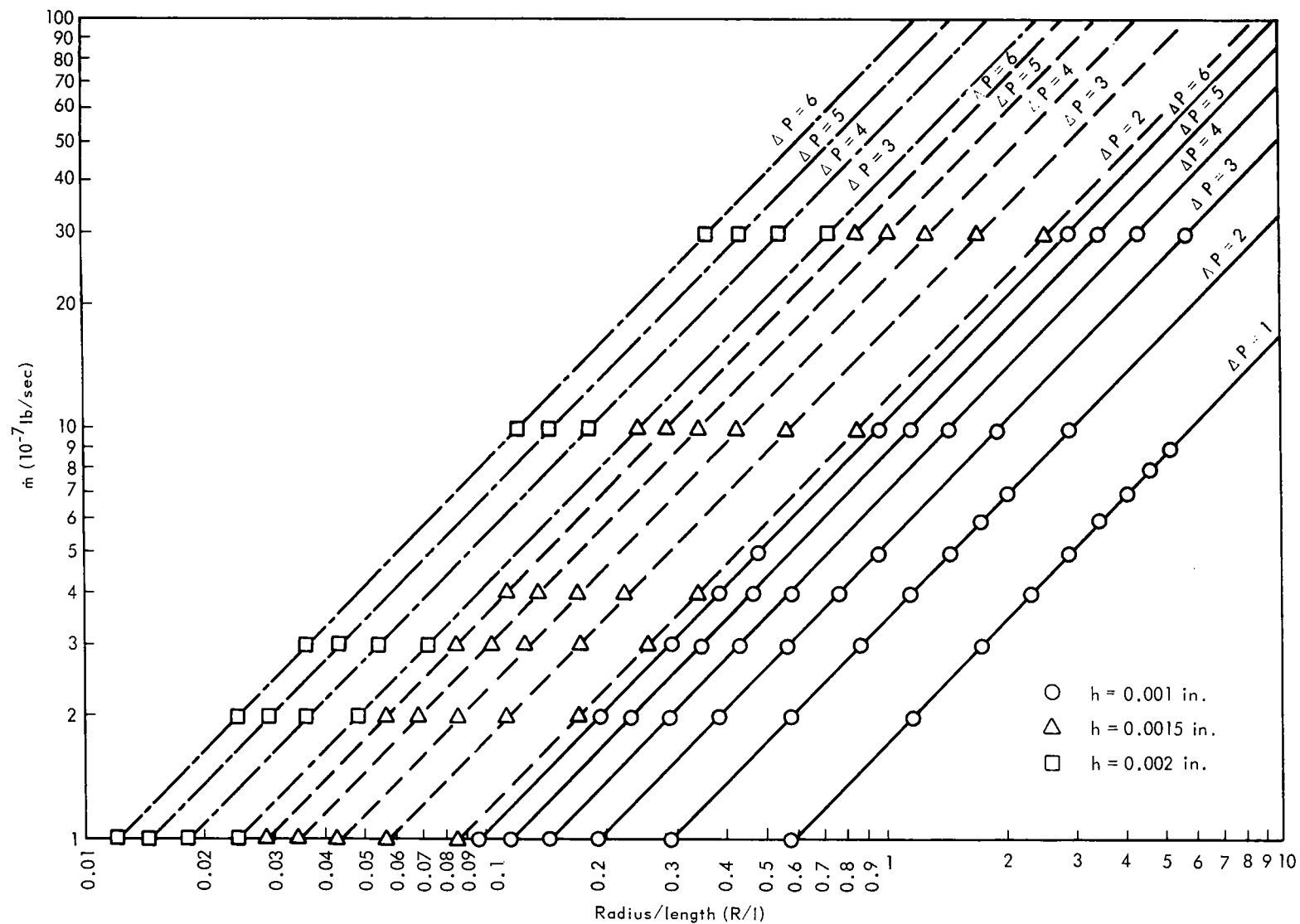


Figure 2— \dot{m} versus R/l for annular slit thruster design. $\dot{m} = \frac{\Delta P \pi R h^3 \rho}{6 \mu l}$, $\mu_{\text{gly}} = 1.383 \times 10^{-7} \text{ lb-sec/in.}^2$, and $\rho_{\text{gly}} = 0.0455 \text{ lb/in.}^3$.

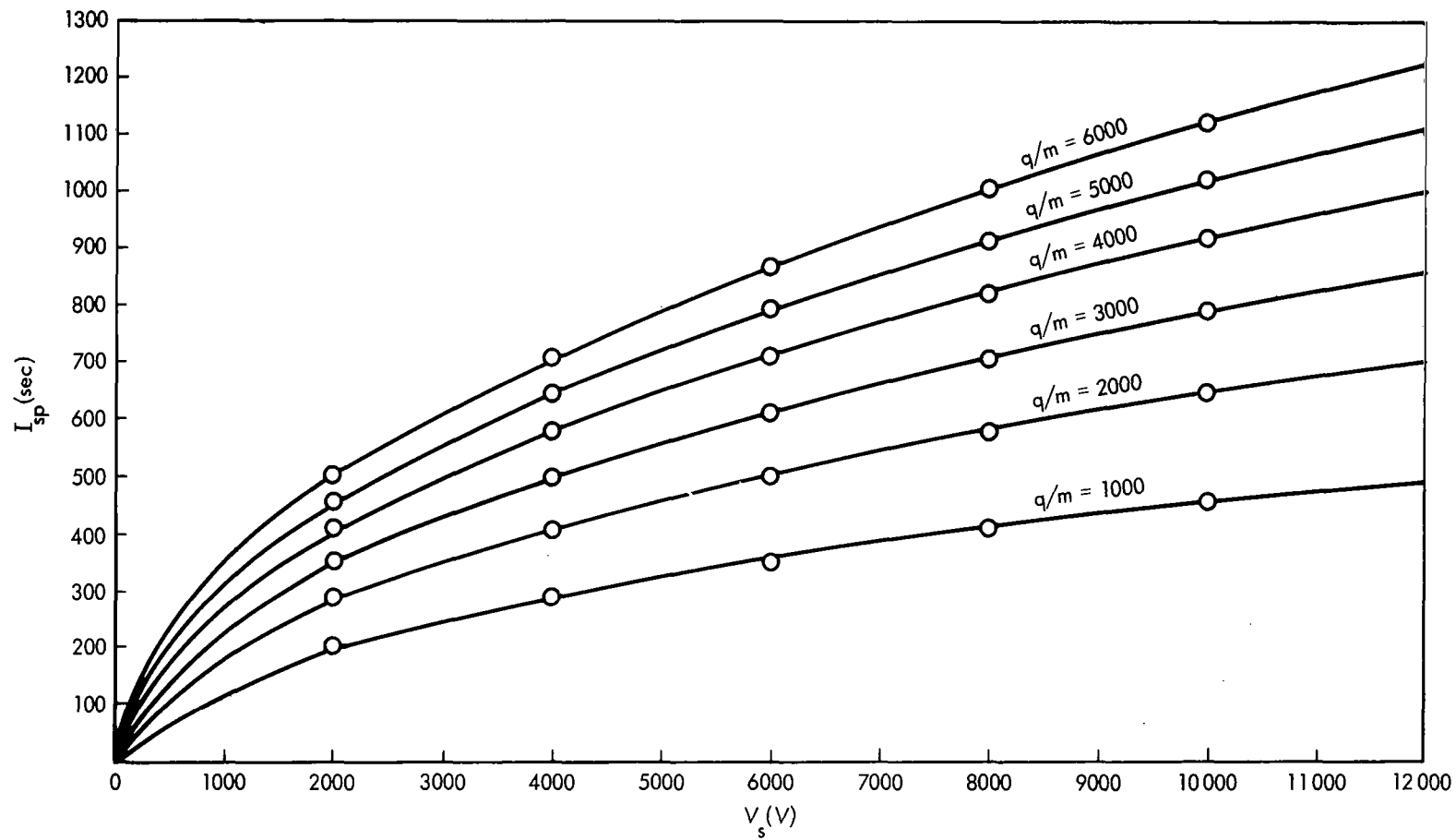


Figure 3— I_{sp} versus source voltage at various q/m 's. $I_{sp} = \frac{4.66}{g_0} \sqrt{q/m \cdot V_s}$, V_s in V, q/m in C/kg, and I_{sp} in sec.

Table 1 — Thruster design parameters.

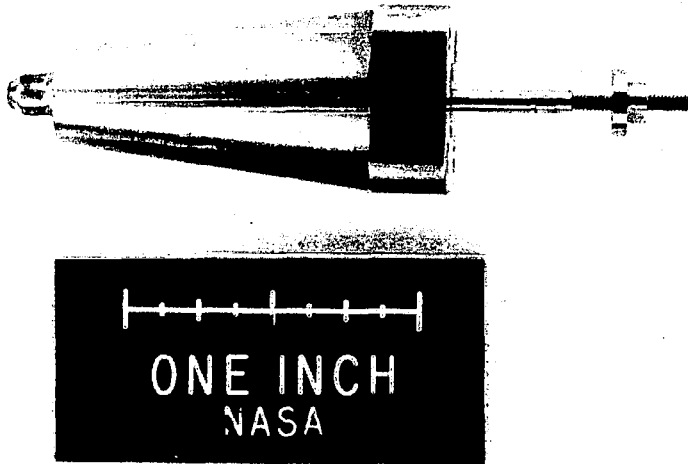
Thruster size	R_1 (in.)	R_2 (in.)	l (in.)	\dot{m}_t (lb/sec)	Material
Small	0.0400	0.0422	1.5	1.6×10^{-7}	20Cb-3 stainless steel
Large	.3800	.3815	1.0	1.11×10^{-6}	20Cb-3 stainless steel



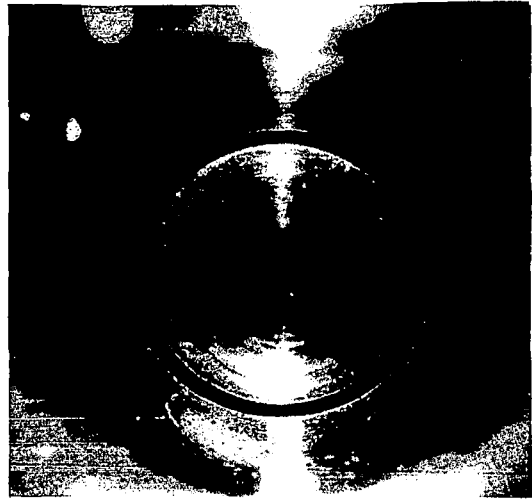
Figure 4—Large annular thruster.

Table 2 — Original performance goals.

Thruster size	I_{sp} (sec)	T_t (μ lb)	q/m (C/kg)
Small	900	144	3000
Large	900	1000	3000



(a)



(b)

Figure 5—Small annular thruster, (a) side view, and (b) front view.

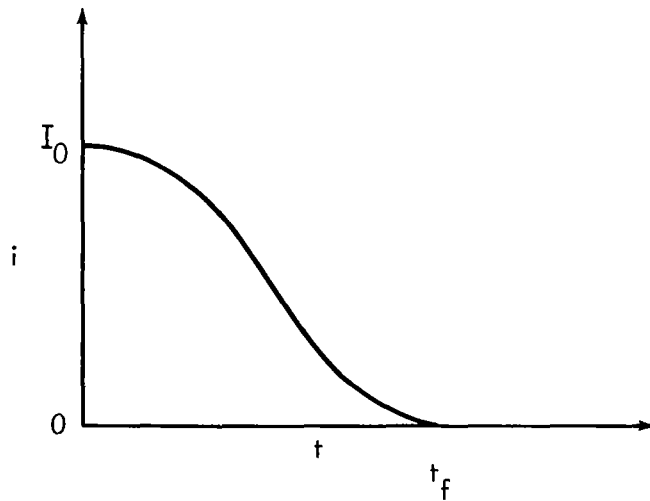


Figure 6—Typical time of flight (TOF) trace.

A computer program was written for the reduction of data obtained from the TOF curves. This program computes the colloid thruster performance parameters from inputs of sets of points of current and time. These points are obtained from enlarged photographs (8 in. by 10 in.) of the original oscilloscope picture (3 in. by 5 in.).

The sets of points are used in the program to evaluate numerically the integrals required for the TOF equations,

$$X_1 = \int_0^{t_f} i \, dt \quad (3)$$

and

$$X_2 = \int_0^{t_f} i \, t \, dt. \quad (4)$$

The numerical method selected for the evaluation of these integrals is Simpson's one-third rule.

Once X_1 and X_2 are calculated, the program computes the test performance parameters by the standard TOF equations.

$$T_c = \frac{2V_s}{d} X_1 \quad (5)$$

$$\dot{m}_c = \frac{4V_s}{d^2} X_2 \quad (6)$$

$$\text{ACMR} = \frac{T_c}{\dot{m}_c} \quad (7)$$

$$\eta_b = \frac{T_c^2}{2V_s I_c \dot{m}_c} \quad (8)$$

$$\eta_b = \frac{q/m}{ACMR} \quad (9)$$

$$I_{sp} = \frac{T_c}{\dot{m}_c g_0} \quad (10)$$

LABORATORY APPARATUS AND TEST PROCEDURE

Horizontal Firing

During the initial series of tests on the annulus thruster, the laboratory test setup was essentially the same as that used with the capillary needles (Reference 2). Figure 7 shows the basic testing apparatus with the collector and thruster mounted in a horizontal position. The feed system shown proved to be satisfactory and was maintained essentially unchanged throughout the annulus testing program.

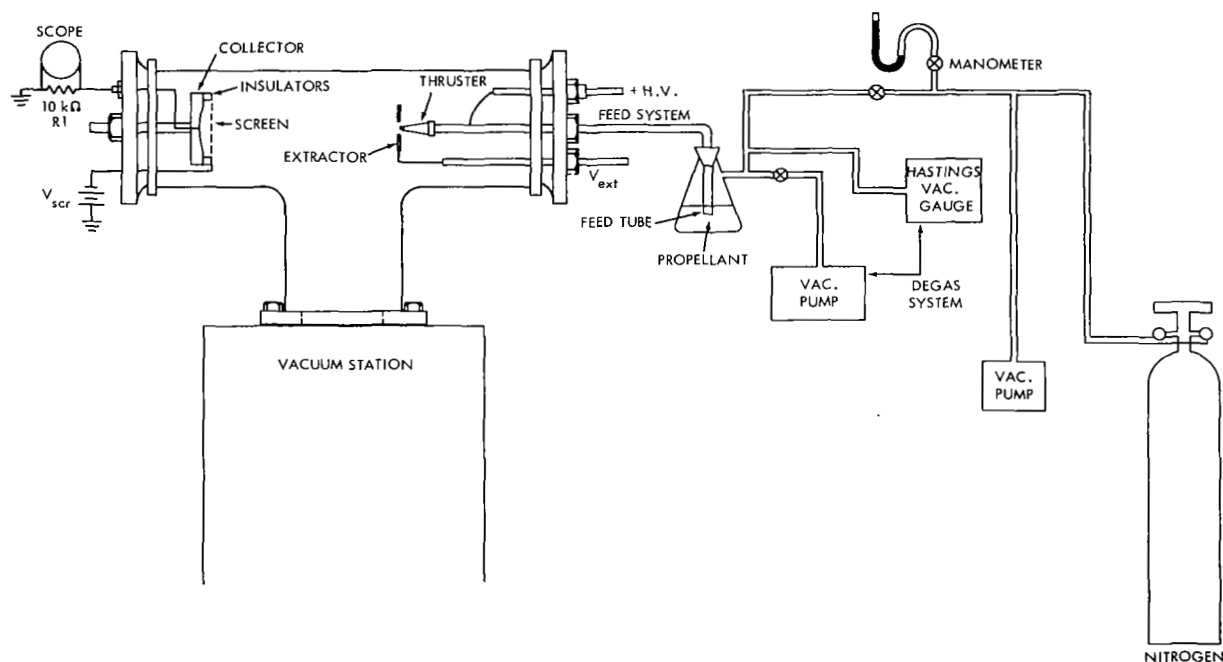


Figure 7—Basic testing apparatus diagram. The collector and the thruster are mounted in a horizontal position.

Initial test data taken with this orientation were characterized by poor q/m and low collector and screen currents relative to input current values. This type of performance indicated poor particle distribution with large beam divergence angles. Further testing showed the beam to be impacting on the lower portion of the collector with deposits of propellant accumulating on the chamber wall below the collector. This evidence indicated that the meniscus and the beam trajectory were being affected by gravitational force because of the horizontal orientation of the thruster. Attempts to focus the beam by incorporating various configurations of focusing electrodes were unsuccessful because of the effects these devices had on field intensity and concentration at the emission site. It was decided at this point that further testing would necessitate a change in the thruster orientation to the vertical.

Vertical Firing Downward

Figure 8 shows the test setup, a cross configuration vacuum chamber with the thruster mounted pointing downward for a vertical firing orientation. Propellant mixture and voltage parameters were essentially the same as in previous tests.

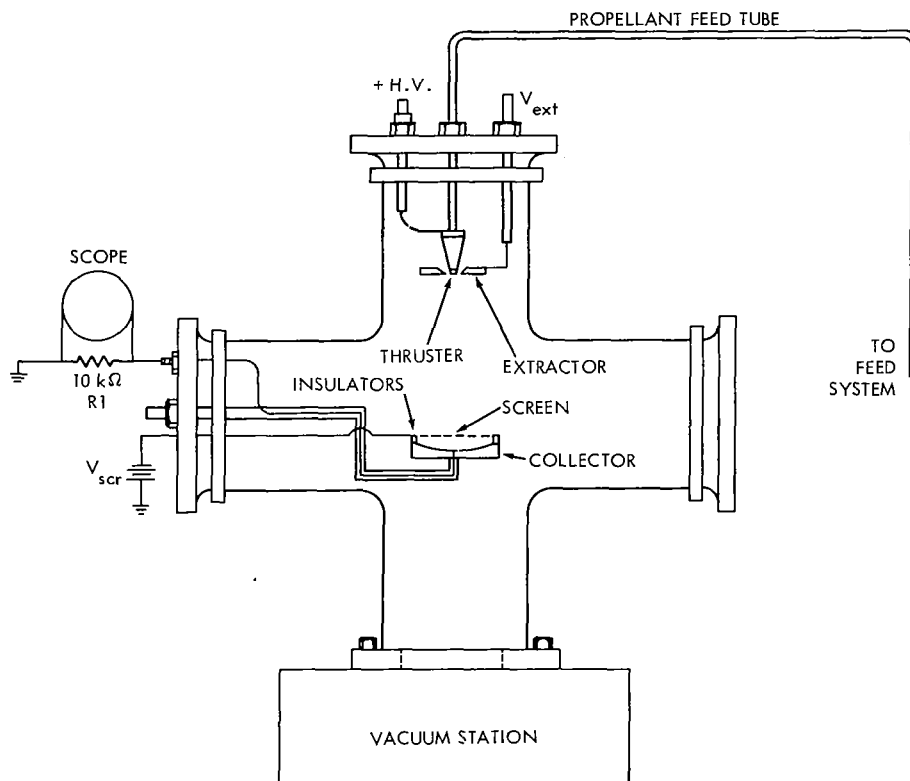


Figure 8—The cross-configuration vacuum chamber. The thruster is mounted in a vertical position.

Preliminary tests showed that excessive arcing and corona discharge occurred in the area of the thruster and extractor, which in turn caused erratic collector currents. It was reasoned that the cause was a buildup of pressure in the area of the thruster. Chamber pressures recorded by the ionization gauge were within permissible limits. However, because of the physical location of the gauge relative to the thruster, these values were not necessarily representative of those at the thruster site. This pressure differential was apparently caused by the accumulation of particles that had rebounded from the collector to the thruster area. These particles were not evacuated efficiently because the collector acted as an obstruction to flow to the vacuum port. Grounded aluminum foil was used on the chamber walls near the beam path in an attempt to collect these particles. The effect was negligible. A screen collector was also tried but proved to be excessively noisy because of external pickup due to the absence of a surrounding shield. It was concluded from these tests that due to the higher flow rates used with the annulus thruster and the relatively low pumping capability of the vacuum system, the thruster should be located as close as possible to the pumping port.

Vertical Firing Upward

A standard bell jar vacuum chamber was used to facilitate vertical firing with the thruster close to the vacuum port (Figure 9). The port was directly below the thruster. Several problems occurred in initial tests with this setup. The portion of the feedline in the chamber that runs parallel with the base plate was bombarded by secondary particles. The bombardment caused localized heating, which affected the propellant viscosity and, in turn, the flow characteristics. This situation was remedied by the installation of a shield for the feedline in this area maintained at the negative extractor potential.

Preliminary TOF traces showed high-amplitude noise spikes and excessive overshoot. After a series of tests it was determined that the thruster collector support rod was not properly grounded, which induced radiative effects. More effective grounding of this rod alleviated the problem.

It was also found that clamps used to attach the thruster and collector to the support rod were arcing badly. Inspection of the clamps showed them to have a nonconductive coating, which apparently caused a charge to build up as they were impacted by the charged particles. The buildup, after reaching a certain level, would discharge through the coating to the grounded conductive core. Replacing these clamps with uncoated ones prevented further arcing.

There were no further problems associated with this test setup, and it was used for the remainder of the test program.

Time of Flight Techniques

Ball Zapper

The term "Zapper," as used in this text, refers to the apparatus used to short the thruster voltage to ground during TOF trace initiation. The original TOF zapper circuit

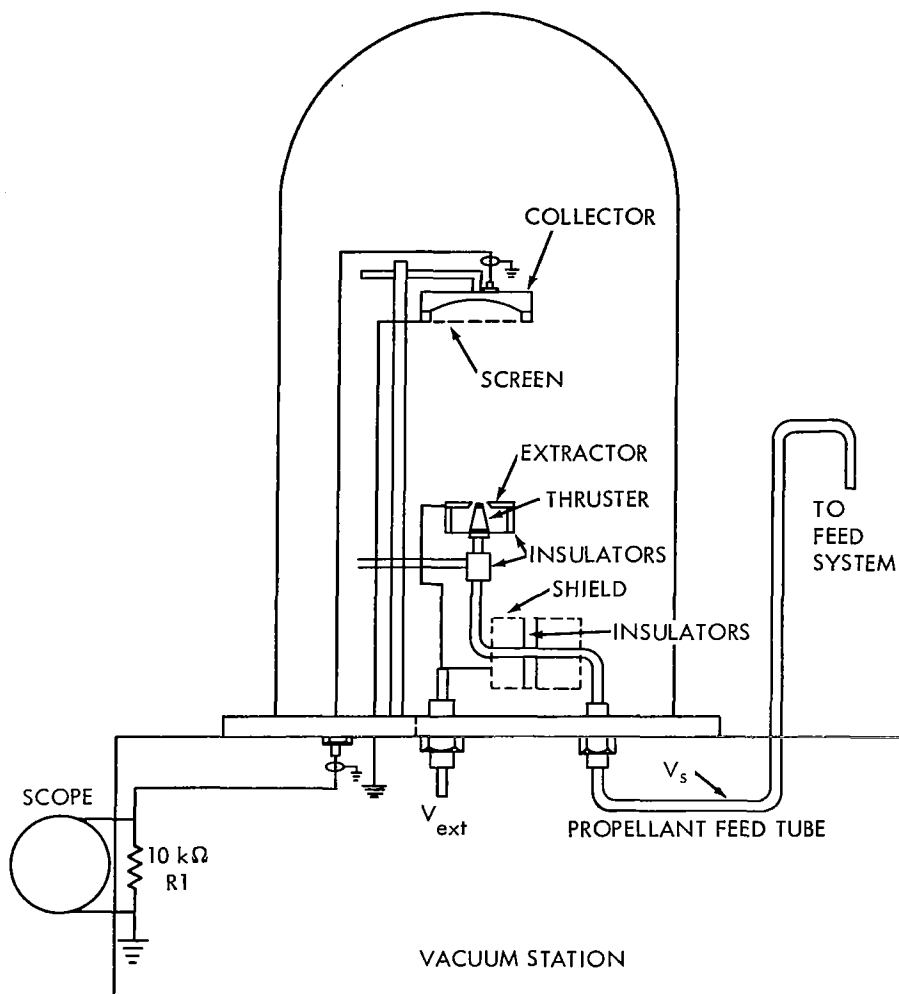


Figure 9—Diagram of the standard bell jar vacuum chamber used to facilitate vertical firing.

is shown schematically in Figure 10. This is a spring-loaded push rod type of mechanical switch that uses stainless steel balls as shorting contacts. Load resistors were incorporated to prevent the high-voltage power supply from being overloaded during shorting. This unit operated satisfactorily as long as collector currents were of a high enough level to maintain oscilloscope input sensitivity at 10 mV/cm or lower. Characteristic TOF "dead times" under these conditions were 7 to 12 μ sec (Figure 11) with a trigger transient apparent. Dead time is defined as the period between shorting the thruster voltage to ground and the beginning of the TOF current decay curve. As oscilloscope input sensitivity was increased above 10 mV/cm, the trigger transient saturated the preamplifier and caused the dead time to increase. Collector currents at this time were of sufficient magnitude to enable the oscilloscope input sensitivity to be maintained at the lower levels. However, in subsequent testing these levels decreased, and it was necessary to devise a more efficient zapping method.

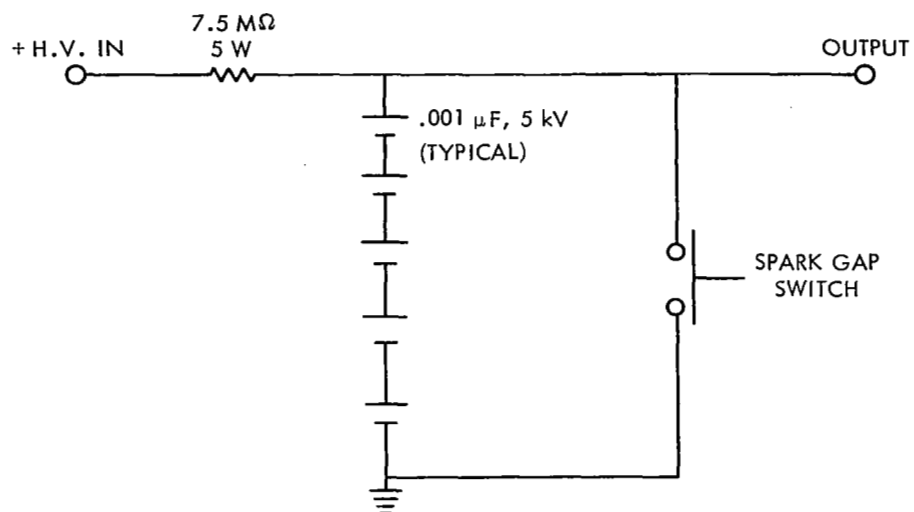


Figure 10—Ball zapper circuit.

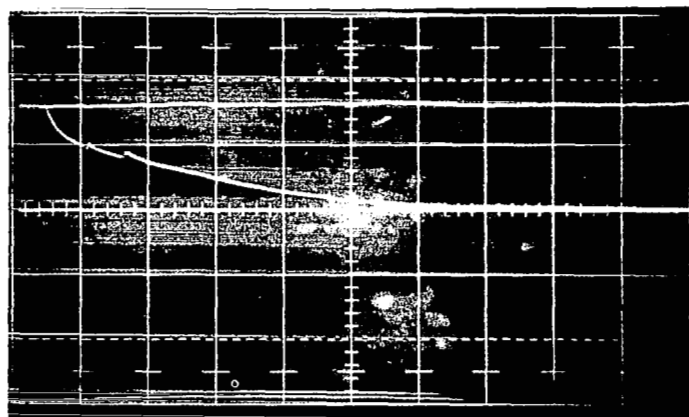


Figure 11—TOF trace of AS-48-2. $V_s = 21.5 \text{ kV}$, $I_s = 140 \text{ μA}$, $i = 10 \text{ μA/cm}$, and the sweep was 20 μsec/cm .

Thyratron Zapper

Figure 12 is a schematic diagram of the final version of the thyratron zapper unit used in the latter stages of testing. Operation of this unit depends on short circuiting the high voltage to ground through the thyratron by biasing the control grid to start conduction. This method of operation eliminates the arcing and consequent radiation associated with the shorting of the high voltage through a mechanical switching device. Essentially, this eliminated the transient effects of the ball zapper previously used, and consequently collector current amplitude ceased to be a major factor in dead time variations. Testing conducted with this zapper unit resulted in TOF traces with dead times of 5 to 10 μsec . Redesign of the collector configuration to permit the collector to be completely surrounded by a grounded shield resulted in further reduction of this dead time to 3 to 5 μsec (Figure 13). The final version of the collector configuration is shown in Figure 14.

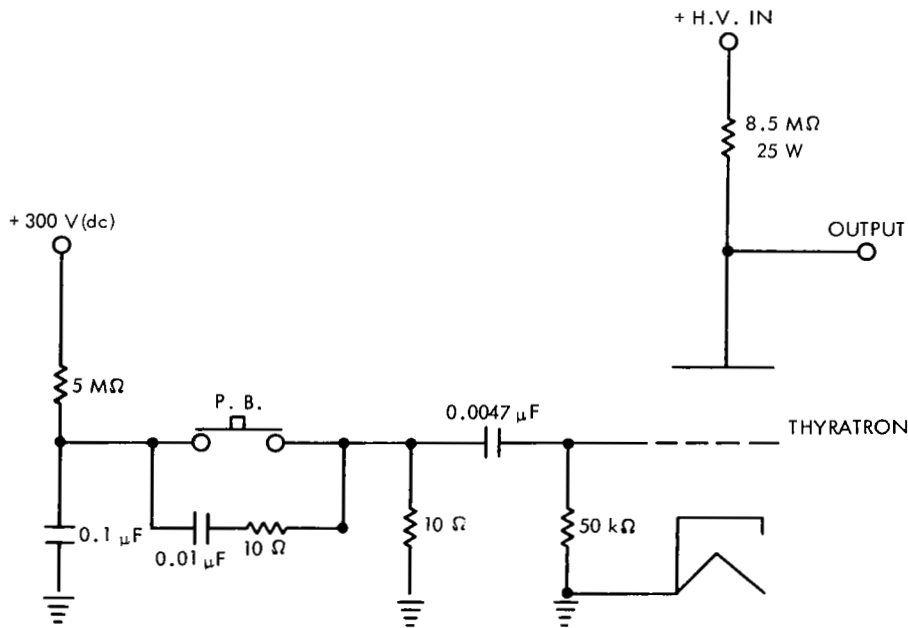


Figure 12—Thyratron zapper circuit.

RESEARCH PROGRAM AND RESULTS

Fifty-eight tests investigating performance, material compatibility, propellant combinations, thruster geometry, test setups, and TOF trace shorting circuits were run. The test setups and TOF circuits have been discussed earlier.

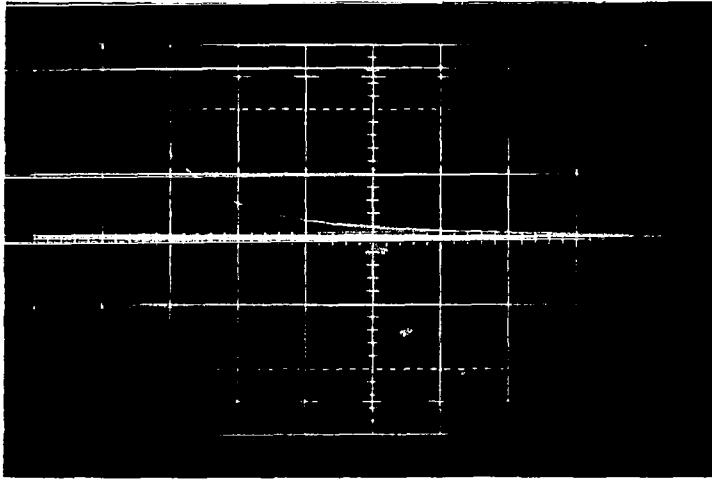


Figure 13—TOF trace of AS-58-2. $V_s = 17.5 \text{ kV}$, $I_s = 100 \text{ } \mu\text{A}$, $i = 5 \text{ } \mu\text{A/cm}$, and the sweep was $10 \text{ } \mu\text{sec/cm}$.

Performance indicated by TOF data reduction are tabulated in Table 3. In tests AS-10 through AS-29 thruster orientation within the vacuum chamber was varied, and several extractor and focusing geometries and other variables were tested.

Rather than describe all the individual debugging tests conducted, the results of these investigations will be listed as they applied to the final conditions under which the majority of tests were conducted. Any variations from these will be pointed out during the discussion of the appropriate test. Generally, tests AS-10 through AS-29 resulted in the remaining tests being conducted under the following conditions:

(1) All metal clamps and holders in the vacuum chamber were conductive without insulating surface coatings.

(2) All fixtures and items necessary to thruster performance inside the thrust chamber were either biased at a given voltage or grounded.

(3) Extractor voltage was set at -2000 V .

(4) The diameter of the aperture in the extractor plate was 0.334 in.

(5) The inner shaft was recessed from 0.002 to 0.005 in. below the outer rim of the thruster.

(6) The thruster operating orientation within the bell jar was vertical, spraying upward.

(7) A gold-plated melamine collector was used through test AS-55. In subsequent tests, a stainless steel collector with grounded screen was used.

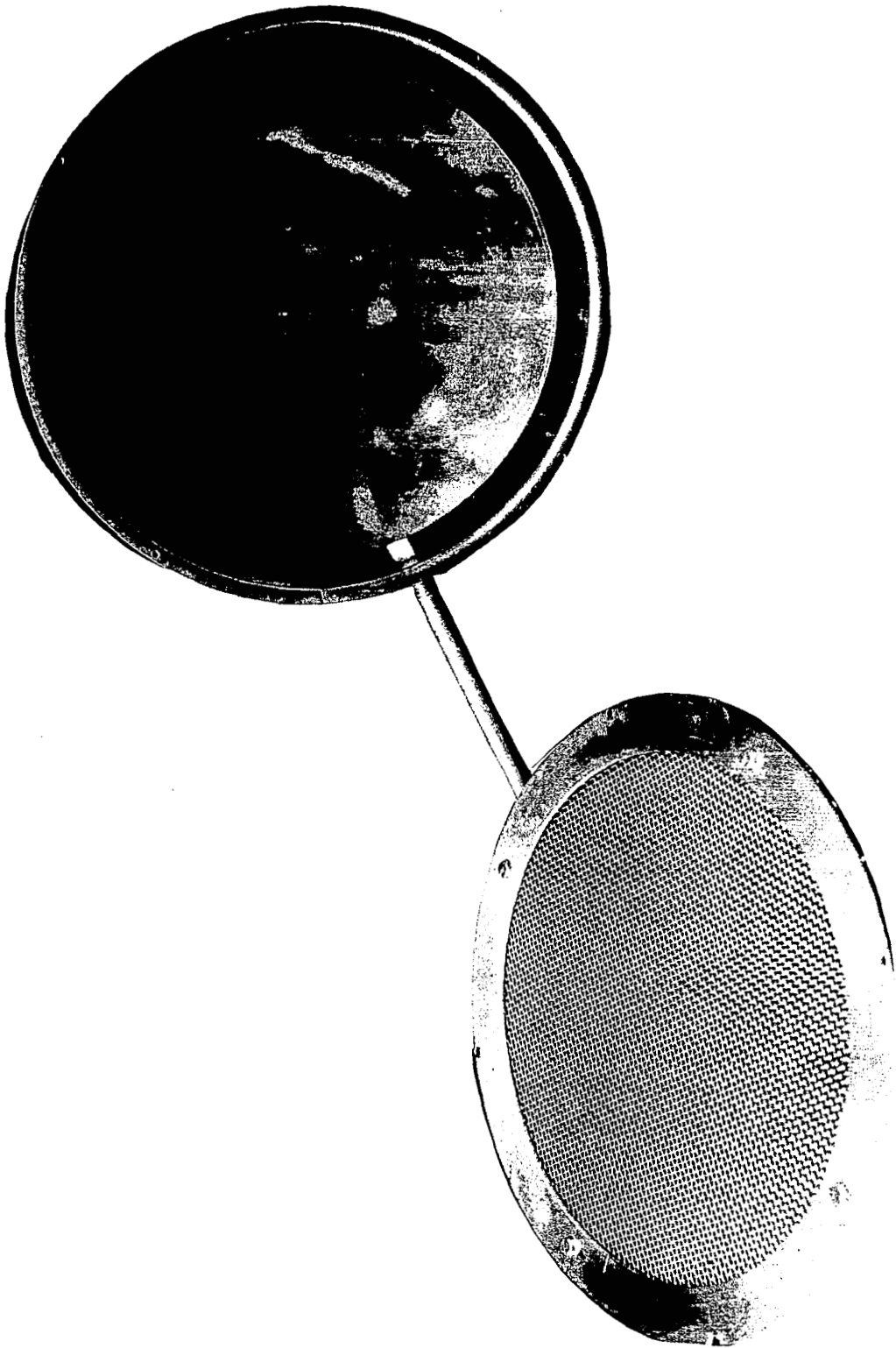


Figure 14—Stainless steel shielded collector assembly.

Table 3 — Summary of AS thruster tests.

Test number	Propellant number	V_g (kV)	V_{ext} (kV)	V_{scr} (V)	I_{scr} (μ A)	I_c (μ A)	I_s (μ A)	I_{ext} (μ A)	ACMR (C/kg)	I_{sp} (sec)	\dot{m}_t (lb/sec)	T_t (μ lb)	η_b (%)	q/η (C/kg)	P_f (mm Hg)	P_{ch} (mm Hg)	Comments
AS-23-1	19	12.5	- .473	-45	-	1.64	10	-	1750	514	$.125 \times 10^{-7}$	6.45	57.8	1010	180	4.7×10^{-5}	Hand-reduced data
AS-26	20	23.5	- .473	-45	-	16	156	2	-	-	-	-	-	-	240	5.5×10^{-5}	-
AS-29-1	20	15	-2	-45	20	2.48	40	-	1590	580	$.552 \times 10^{-7}$	32	67.3	1070	60	1.6×10^{-5}	-
AS-30-4	20	16.25	-2	+45	80	60	250	5.5	2565	722	2.15×10^{-7}	155	60.6	1555	85	3.4×10^{-5}	Evaluation of $\pm V_{scr}$
AS-30-5	20	16.25	-2	-45	130	14.1	250	5.0	2604	698	2.12×10^{-7}	149	55.9	1455	85	3.4×10^{-5}	Evaluation of $\pm V_{scr}$
AS-30-13	20	17.75	-2	+45	125	85	400	-	2455	753	3.59×10^{-7}	270	63.0	1547	85	3.4×10^{-5}	Evaluation of $\pm V_{scr}$
AS-30-14	20	17.75	-2	-45	220	20	375	-	1447	553	5.7×10^{-7}	316	57.7	835	85	3.4×10^{-5}	Evaluation of $\pm V_{scr}$
AS-31-1	20	18	-2	+45	100	85	275	4	6286	1239	$.965 \times 10^{-7}$	119	65.7	4132	60	2.6×10^{-5}	•
AS-31-2	20	18	-2	+45	80	70	225	4	4590	1041	1.08×10^{-7}	113	63.5	2916	60	2.8×10^{-5}	*
AS-31-3	20	18	-2	+45	80	70	230	4	4265	902	1.18×10^{-7}	107	51.4	2192	60	3.2×10^{-5}	*
AS-31-4	20	18	-2	+45	95	80	250	4	3160	821	1.74×10^{-7}	143	57.4	1813	60	4.0×10^{-5}	•
AS-31-5	20	18	-2	+45	95	80	260	4	3968	908	1.44×10^{-7}	131	56.0	2222	60	5.2×10^{-5}	*
AS-31-6	20	18	-2	+45	95	82.5	250	4	2671	691	2.06×10^{-7}	143	48.0	1285	60	4.0×10^{-5}	•
AS-31-8	20	18	-2	-	-	160	230	5.5	1863	620	2.72×10^{-7}	168	55.6	1035	60	4.0×10^{-5}	Screen and collector connected
AS-31-10	20	17	-2	+45	60	50	180	5.5	2141	631	1.85×10^{-7}	117	53.0	1136	60	3.0×10^{-5}	V_g variation test
AS-31-11	20	16	-2	+45	45	32	130	8.0	1262	452	2.27×10^{-7}	102	49.0	620	60	2.6×10^{-5}	V_g variation test
AS-31-12	20	15	-2	+45	20	14	70	5.0	1163	390	1.33×10^{-7}	52	42.4	493	60	2.2×10^{-5}	V_g variation test
AS-31-13	20	14	-2	+45	8	6.15	50	2	907	389	1.21×10^{-7}	47	57.6	523	60	2.0×10^{-5}	V_g variation test
AS-31-14	20	13	-2	+45	1.5	1.49	30	1	891	347	$.74 \times 10^{-7}$	26	50.4	449	60	1.9×10^{-5}	V_g variation test
AS-32-1b	20	18	-2	+45	40	39	110	2	2258	718	1.07×10^{-7}	77	61.4	1386	60	2×10^{-5}	Test of 0.001-in. focuser*
AS-32-2	20	18	-2	+45	40	36	100	2	2430	753	$.905 \times 10^{-7}$	69	62.9	1528	60	2×10^{-5}	Test of 0.001-in. focuser*
AS-32-3	20	18	-2	+45	40	33	100	2	1808	628	1.22×10^{-7}	77	58.7	1061	60	2.2×10^{-5}	Test of 0.001-in. focuser*
AS-32-4	20	18	-2	+45	40	35	100	2	1853	627	1.19×10^{-7}	75	57.0	1058	60	2.2×10^{-5}	Test of 0.001-in. focuser*
AS-32-5	20	18	-2	+45	45	42	125	2	1794	610	1.53×10^{-7}	94	55.8	1001	60	2.2×10^{-5}	Test of 0.001-in. focuser*
AS-32-6	20	18	-2	+45	45	39	125	2	1989	672	1.38×10^{-7}	93	61.1	1215	60	2.4×10^{-5}	Test of 0.001-in. focuser*
AS-32-8	20	18	-2	+90	45	40	130	2	2053	672	1.4×10^{-7}	94	59.1	1214	60	2.4×10^{-5}	Run at $V_{scr} = 90$ V
AS-33-1	20	18	-2	+45	85	82.5	230	2	4298	963	1.18×10^{-7}	113	58.1	2499	60	2.4×10^{-5}	†

* 5-hour duration test—points taken at 1-hour intervals.

† 4-hour duration test—points taken at 1-hour intervals.

Table 3 — Summary of AS thruster tests (Con.)

Test number	Propellant number	V_s (kV)	V_{ext} (kV)	V_{scr} (V)	I_{scr} (μ A)	I_o (μ A)	I_s (μ A)	I_{ext} (μ A)	ACMR (C/kg)	I_{sp} (sec)	\dot{m}_t (lb/sec)	T_t (μ lb)	η_b (%)	q/m (C/kg)	P_f (mm Hg)	P_{ch} (mm Hg)	Comments
AS-33-2g	20	18	-2	+45	110	102.5	300	4	3793	819	1.75×10^{-7}	143	47.6	1808	60	3×10^{-5}	†
AS-33-3	20	18	-2	+45	110	102.5	300	4	3979	899	1.66×10^{-7}	150	54.6	2175	60	3.4×10^{-5}	†
AS-33-4d	20	18	-2	+45	105	90	280	4.5	4012	873	1.54×10^{-7}	134	51.1	2052	60	3.8×10^{-5}	†
AS-33-5	20	18	-2	+45	115	100	300	6.0	3742	853	1.77×10^{-7}	150	52.3	1957	60	3.4×10^{-5}	†
AS-33-7	20	16	-2	+45	45	39.5	140	4	3806	888	$.814 \times 10^{-7}$	72	62.7	2386	60	4×10^{-5}	V_s variation test points
AS-33-8	20	17	-2	+45	90	72.5	250	5	3018	738	1.82×10^{-7}	135	51.4	1550	60	4×10^{-5}	V_s variation test points
AS-33-9	20	18	-2	+45	115	102.5	340	6	4426	924	1.7×10^{-7}	157	51.9	2298	60	4.2×10^{-5}	V_s variation test points
AS-33-10	20	19	-2	+45	150	102.5	400	8	4297	895	2.06×10^{-7}	184	47.5	2041	60	4.2×10^{-5}	V_s variation test points
AS-33-11	20	20	-2	+45	170	122.5	450	9	4054	892	2.45×10^{-7}	218	47.5	1926	60	4.4×10^{-5}	V_s variation test points also glow spray observed
AS-33-13	20	18	-2	+45	-	92.5	300	-	3493	853	1.9×10^{-7}	161	56.0	1956	60	-	P_f variation test points
AS-33-14	20	18	-2	+45	-	82.5	300	-	1423	496	4.65×10^{-7}	230	46.6	663	135	-	P_f variation test points
AS-35-1	21	16.75	-2	+45	90	60	310	3	4071	932	1.68×10^{-7}	157	61.8	2514	60	3×10^{-5}	**
AS-35-2	21	15.75	-2	+45	85	60.5	300	10	3698	852	1.79×10^{-7}	152	60.4	2232	60	3.2×10^{-5}	**
AS-35-3	21	16.25	-2	+45	85	62.5	250	10	4091	914	1.35×10^{-7}	123	60.9	2492	60	3×10^{-5}	**
AS-35-4	21	16.5	-2	+45	85	60	250	8	4407	950	1.25×10^{-7}	119	60.2	2652	60	3×10^{-5}	**
AS-35-5	21	16.25	-2	+45	80	60	270	7	4325	973	1.38×10^{-7}	134	65.2	2820	60	3.4×10^{-5}	**
AS-35-6	21	17.5	-2	+45	65	38	210	6	2953	741	1.57×10^{-7}	116	51.5	1519	60	2.2×10^{-5}	**
AS-35-7	21	18	-2	+45	110	72.5	330	8	5327	1053	1.37×10^{-7}	144	56.0	2982	60	3.4×10^{-5}	**
AS-35-8	21	17	-2	+45	80	41	250	8	5000	843	1.1×10^{-7}	93	40.5	2026	60	4×10^{-5}	**
AS-35-9	21	17	-2	+45	80	60	250	10	7511	1166	$.735 \times 10^{-7}$	86	51.6	3876	60	3.6×10^{-5}	* also glow spray
AS-35-11	21	16.5	-2	+45	80	46	230	12	6489	1153	$.781 \times 10^{-7}$	90	60.0	3901	60	3.8×10^{-5}	also glow spray
AS-35-12	21	16.75	-2	+45	80	50	300	16	14 280	1745	$.463 \times 10^{-7}$	81	61.7	8807	60	4.2×10^{-5}	also glow spray
AS-35-13	21	16.5	-2	+45	80	50	325	20	21 520	2265	$.332 \times 10^{-7}$	76	70	15 060	60	4.8×10^{-5}	* also glow spray
AS-35-14	21	18	-2	+45	90	50	350	22	17 870	2113	$.432 \times 10^{-7}$	91	67.3	12 020	60	4.6×10^{-5}	also glow spray
AS-35-16	21	17	-2	+45	85	50	270	26	19 750	2188	$.302 \times 10^{-7}$	66	69.1	13 640	60	4×10^{-5}	also glow spray
AS-35-17	21	18	-2	+45	175	102.5	570	50	9896	1257	1.27×10^{-7}	160	43.0	4255	60	7×10^{-5}	also glow spray
AS-35-18	21	17.5	-2	+45	175	115	600	60	16 400	1842	$.81 \times 10^{-7}$	149	57.3	9394	80	7.2×10^{-5}	* also glow spray

† 4-hour duration test—points taken at 1-hour intervals.

** 120-hour duration test—points taken at random times.

Table 3 — Summary of AS thruster tests (Concluded)

Test number	Propellant number	V_s (kV)	V_{ext} (kV)	V_{scr} (V)	i_{scr} (μA)	I_o (μA)	i_s (μA)	I_{ext} (μA)	ACMR (C/kg)	i_{sp} (sec)	\dot{m} (lb/sec)	T_e (°lb)	η_p (%)	g/η (C/kg)	P_f (mm Hg)	P_{ch} (mm Hg)	Comments
AS-35-19	21	17	-2	+45	170	125	600	65	16880	1864	$.781 \times 10^{-7}$	146	58.7	9899	100	7×10^{-5}	* * also glow spray
AS-35-20	21	18	-2	+45	170	115	650	60	21380	2309	$.674 \times 10^{-7}$	155	67.2	14350	120	8×10^{-5}	* * also glow spray
AS-35-21	21	15.5	-2	+45	200	147.5	725	76	25900	2071	$.62 \times 10^{-7}$	128	51.8	13410	200	8.8×10^{-5}	* * also glow spray
AS-37	22	15	-2	+45	-	14	200	-	300	220	14.6×10^{-7}	323	51.6	155	60	3×10^{-5}	* * * hand-reduced data
AS-42-1	22	14	-2	+45	30	21.5	100	30	700	356	3.15×10^{-7}	112	62.7	439	65	3×10^{-5}	Returned to 30° tapered thruster
AS-42-2	22	14.25	-2	+45	50	25.5	100	50	796	380	2.77×10^{-7}	106	61.8	492	65	3×10^{-5}	Returned to 30° tapered thruster
AS-42-3	22	14.75	-2	+45	50	37	160	50	1172	472	3.01×10^{-7}	142	62.5	732	65	3.8×10^{-5}	Returned to 30° tapered thruster
AS-42-4	22	15.25	-2	+45	70	52	250	70	1905	627	2.89×10^{-7}	181	65.5	1247	65	4×10^{-5}	Returned to 30° tapered thruster
AS-45-1	1	19	-2	+45	-	7.2	75	-	67.5	134	24.5×10^{-7}	329	67.5	45.6	120	2×10^{-5}	Hand-reduced data
AS-46-1	2	19.25	-2	+45	27	27	100	-	440	334	5×10^{-7}	167	63.7	280	-	2.4×10^{-5}	-
AS-46-2	2	20.25	-2	+45	30	32.8	100	-	556	371	3.97×10^{-7}	147	59.3	329	-	2.7×10^{-5}	-
AS-46-4	2	18.5	-2	+45	52	42.8	200	-	567	367	7.75×10^{-7}	284	62.1	352	-	5.2×10^{-5}	-
AS-46-5	2	18	-2	+45	-	50	230	-	5738	1168	$.885 \times 10^{-7}$	103	64.0	3672	-	5×10^{-5}	Glow spray, thruster at 150° F
AS-47-4	3	20	-2	+45	-	11.5	75	-	266	233	6.2×10^{-7}	145	49.4	131	75	2×10^{-5}	-
AS-48-2	5	21.5	-2	+45	18	16.3	140	-	312	295	9.9×10^{-7}	292	62.7	196	96	3.2×10^{-5}	Thruster hot, severe erosion
AS-50-1	11	19.5	-2	+39	-	3.29	50	-	41.9	102	26.2×10^{-7}	267	61.6	25.8	180	1.4×10^{-5}	-
AS-52-1	9	22	-2	+39	-	1.98	30	-	56.0	128	11.8×10^{-7}	151	64.5	36.2	180	$.76 \times 10^{-5}$	-
AS-53-5	16	15.25	-2	+45	10	7.25	50	-	1950	705	$.563 \times 10^{-7}$	39.8	80.9	1577	100	1.5×10^{-5}	-
AS-54-2	23	19.75	-2	+45	9	9.5	50	-	609	369	1.81×10^{-7}	67.0	54.7	334	150	4.8×10^{-5}	-
AS-54-3	23	18.25	-2	+45	20	22.5	125	-	658	367	4.18×10^{-7}	154	54.4	358	140	6×10^{-5}	Glow spray observed
AS-55-1	23	18.75	-2	+45	1	.806	15	-	432	366	$.765 \times 10^{-7}$	28	80.0	345	115	$.4 \times 10^{-5}$	-
AS-55-3	23	16	-2	+45	.2	.175	5	-	168	228	$.655 \times 10^{-7}$	15	93.6	158	115	$.3 \times 10^{-5}$	-
AS-56-1	23	19	-2	-	-	3.2	60	-	2607	774	$.505 \times 10^{-7}$	39	58.6	1528	320	1.6×10^{-5}	First test using large thruster
AS-57-2	23	19	-3	-	-	2.0	45	-	130	172	7.65×10^{-7}	132	58.2	75	100	10×10^{-5}	Positive focuser
AS-58-1	16	15.5	-2	-	-	6.8	50	-	1575	575	$.7 \times 10^{-7}$	40	65.7	1034	100	2×10^{-5}	-
AS-58-2	16	17.5	-2	-	-	12.9	100	-	1597	649	1.38×10^{-7}	90	72.9	1165	100	3.5×10^{-5}	-
AS-58-3	16	16	-2	-	-	21.5	270	7	1278	473	4.65×10^{-7}	220	52.9	676	Clamped	6.2×10^{-5}	Dull glow spray
AS-58-4	16	17	-2	-	-	29.0	350	15	775	379	9.95×10^{-7}	376	52.7	409	115	8×10^{-5}	Glow spray

* * .120-hour duration test—points taken at random times.

* * * 0.0017-in. gap and 15° tapered thruster tested.

(8) The screen was biased at +45 V through test AS-55.

(9) A ball zapper circuit was used through test AS-55. Subsequently, a thyatron zapper circuit was used.

(10) The thruster was unplated 20Cb-3 stainless steel up through test AS-48.

Of the 10 conditions listed above, the eighth needs to be further explained. Normally the screen is biased at a negative voltage to suppress secondary electrons emitted from the collector upon impact by a colloid particle. This biasing prevents fictitiously high collector currents and electron bombardment of the thruster. However, during test AS-29 it was observed that I_C decreased and eventually went negative when V_S was raised above 15 kV and when V_{scr} was lowered from -45 V to -90 V. A possible explanation is that as V_S is increased, particle velocity is increased. These higher energy particles release more electrons upon impact at the screen and collector. Therefore, if the net flow of electrons is increased towards the collector, I_C is reduced. This is very probable because the collector is positive with respect to the screen. Also, as V_{scr} is biased further negatively, the collector appears more positive with respect to the screen and thus attracts more electrons.

It was theorized that if V_{scr} were positive, there should be no problem with negative I_C 's due to reversed electron flow.

Test AS-30 was conducted to determine the effect of positive V_{scr} on performance. Figures 15 and 16 are plots of current variations as V_{scr} is varied from -90 V to +90 V for source voltages of 16.25 kV and 17.75 kV. In both figures, as V_{scr} approaches -90 V, I_C goes to zero or negative current. When TOF traces were attempted in this regime, excessive noise made acceptable TOF traces impossible. However, as V_{scr} was varied between ground and +90 V, I_C remained constant. In both figures the sum of I_{scr} and I_C varies approximately 20% of its maximum value from -90 V to +90 V of V_{scr} . However, the difference between $I_{scr} + I_C$ taken at V_{scr} of +45 V and -45 V was 7% in figure 15 and 2% in Figure 16. At these points, the comparison TOF traces were taken. In both figures I_S drops off at each extreme of the V_{scr} variation. A possible explanation for this is that in the -45 V to -90 V V_{scr} range, the number of electrons that normally would leave the screen and collector to impact on the positive feed-line and thruster is reduced. Also, in the +67 V to +90 V V_{scr} range, it is possible that some of the positive charges are repelled to the feed system, which causes a slight current reduction.

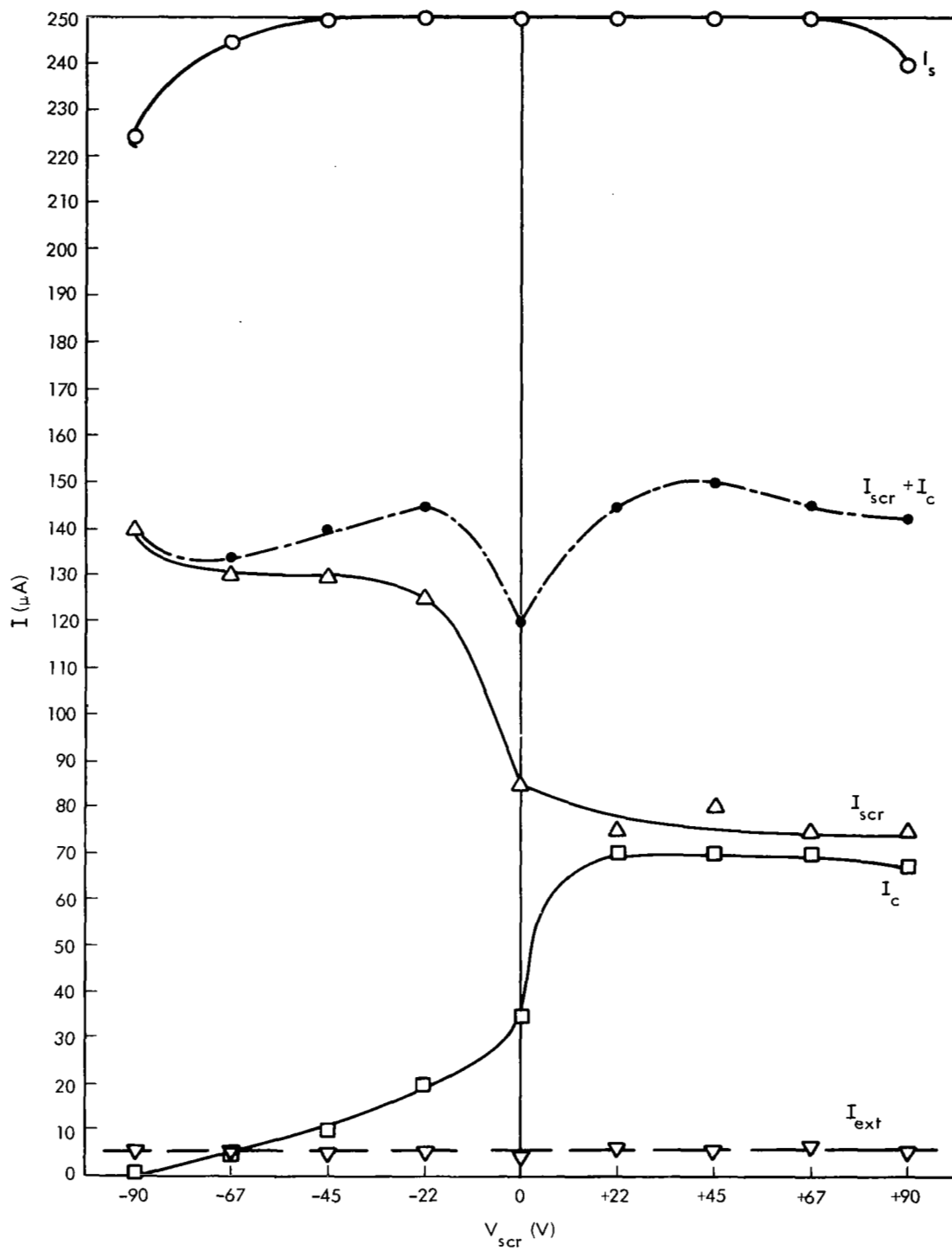


Figure 15—Current variations versus V_{scr} for AS-30 at $V_s = 16.250$ V.

In addition, TOF traces were taken at a V_{scr} of +45 V and -45 V to determine the effect on performance. Data from test points AS-30-4, 30-5, 30-13, and 30-14 are tabulated in Table 3.

If one considers the V_{scr} extremes at which these data were taken, the results are not unlike the variations observed in performance under constant operating conditions.

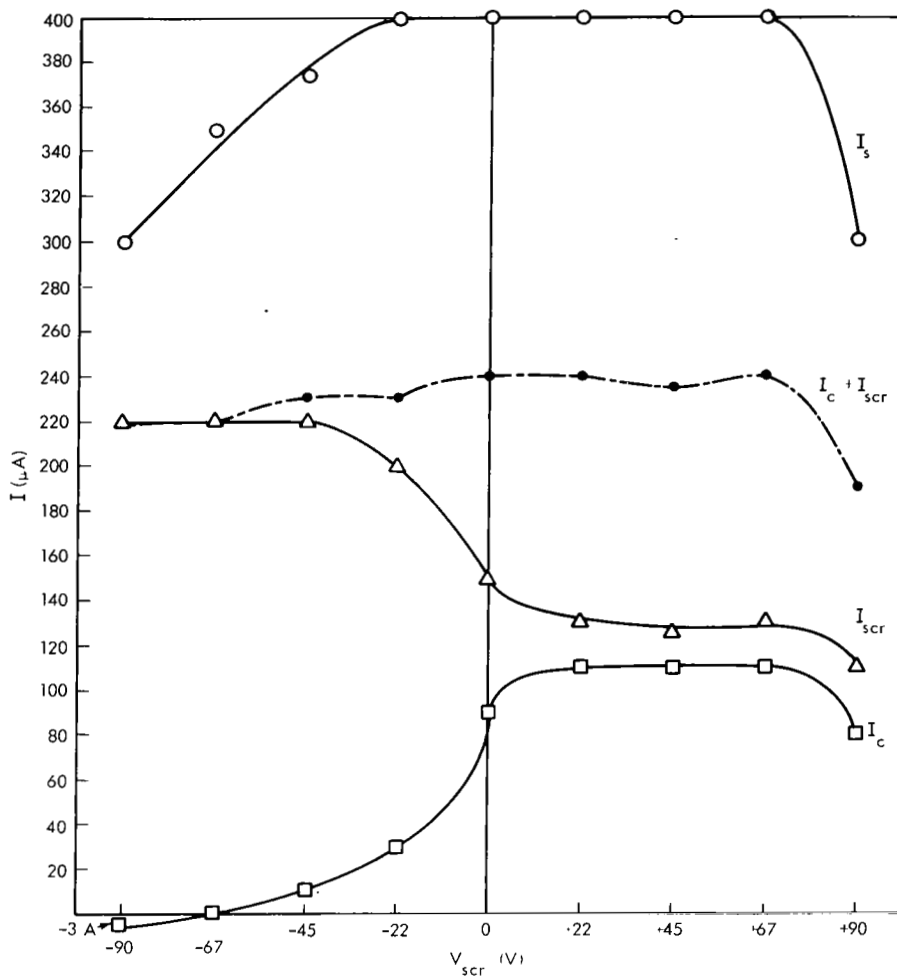


Figure 16—Current variations versus V_{scr} for AS-30 at $V_s = 17.750$ V.

Thruster Performance Testing

Tests AS-31 through AS-35 were conducted for the purpose of thruster evaluation.

Test points AS-31-1 through 31-6 were taken 1 hour apart during a continuous performance of 5 hours. It was observed for the first time that both the screen and collector glowed, although glow spray from the thruster was not seen. Test point AS-31-8 was taken with the collector and screen joined together electrically. Points AS-31-10 through 31-14 were taken at 1-kV decrements of V_S . At 13 kV both I_C and I_{scr} were erratic. During this last set there was no noticeable screen or collector glow. Examination of the thruster after the run showed no erosion (Figure 17).

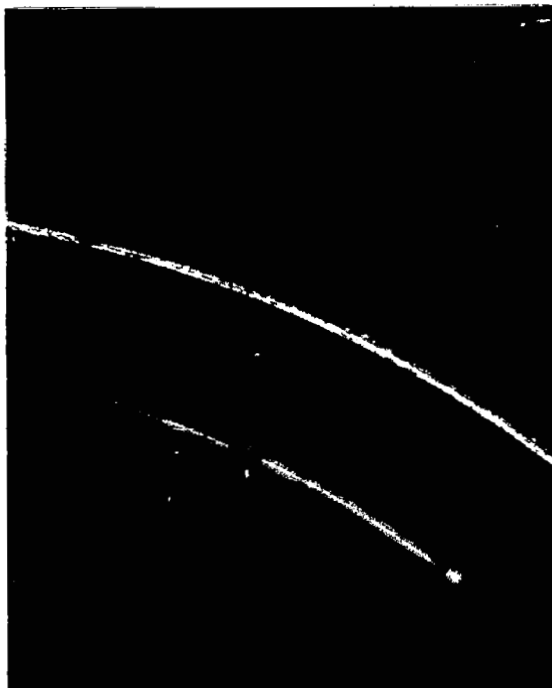


Figure 17—Annular rims after AS-31.

Test AS-32 was conducted in an attempt to reduce the I_S/I_C ratio, which would imply improved beam focusing. Figure 18 depicts the focusing arrangement used. Test points 32-1 through 32-6 were taken, and the reduced data showed a slight improvement in the current ratio (Figure 19). However, a decided reduction in overall performance resulted (Figure 20). Test point 32-8 was operated at $V_{scr} = +90$ V with essentially the same performance as test point 32-6.

Test AS-33 was conducted for two reasons: The first was to see the effect of V_S variation on performance; the second, to see how well the thruster would perform during a 4-hour test. Test points 33-1 to 33-5 were taken 1 hour apart during the operation.

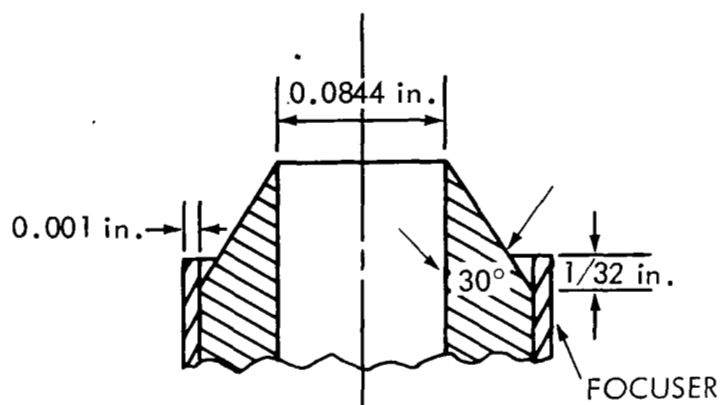


Figure 18-Focuser used for AS-32.

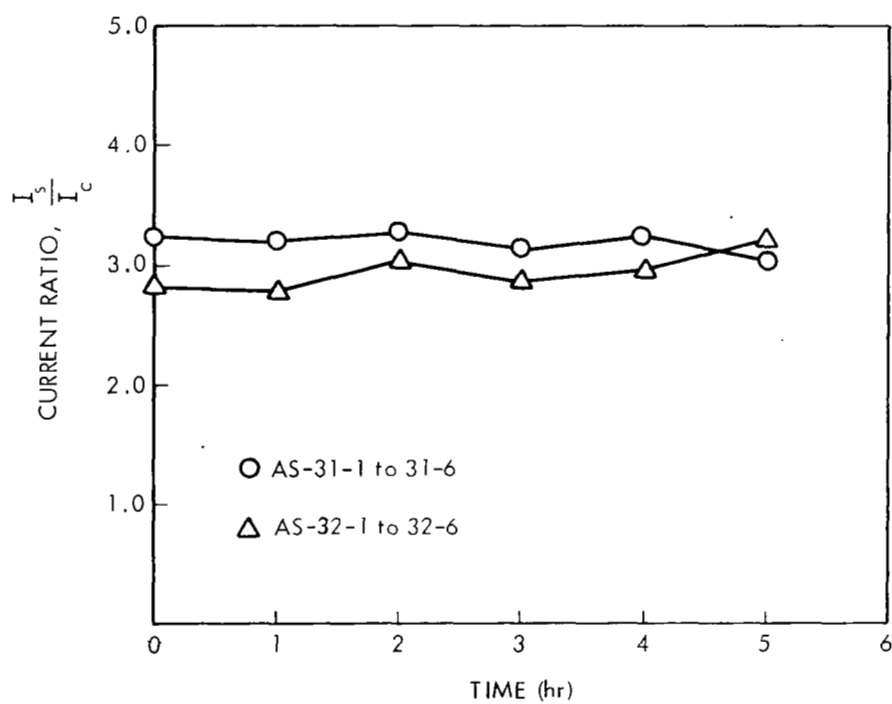


Figure 19-Current ratio versus time. $V_s = 18$ kV, $V_{ext} = -2$ kV, and $V_{scr} = +45$ V.

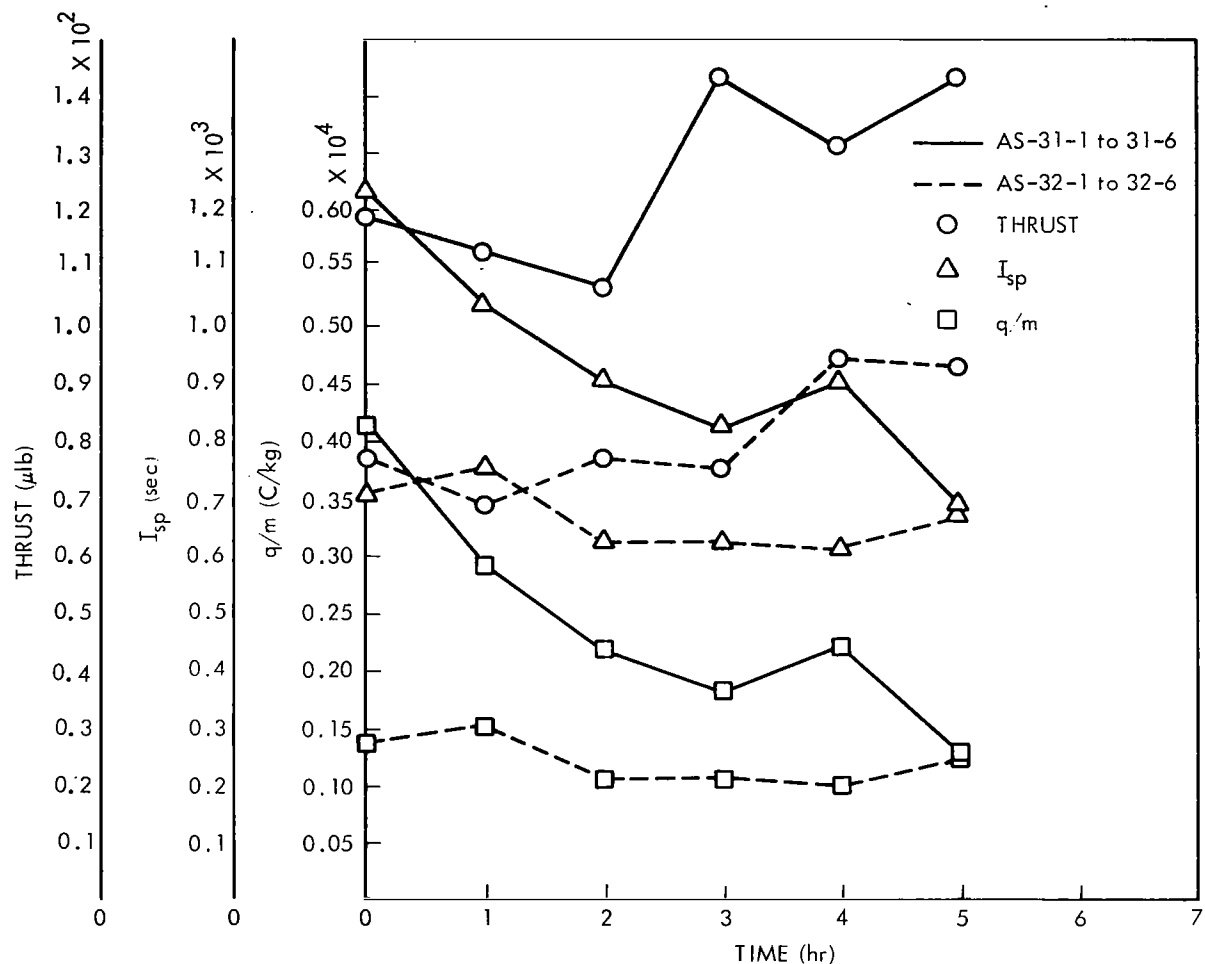


Figure 20—Performance curves versus time. $V_s = 18$ kV, $V_{ext} = -2$ kV, $V_{scr} = +45$ V, and propellant No. 20 was used.

As can be seen from Figure 21, the ratio of source to collector currents is slightly less than 3 during this time, which indicates good focusing. The performance during this time is shown in Figure 22 and is relatively stable. Data from the V_s variation test points are plotted in Figures 23 and 24. An interesting relationship between V_s , I_s , and $I_C + I_{scr}$ is shown in Figure 23. As V_s is increased, I_s and $I_C + I_{scr}$ rise almost linearly; however, when compared to the performance curves in Figure 24, the only effect appears to be an increased flow rate, which resulted in increased thrust. Another important result of the V_s variation shows that the ratio I_s/I_C remained fairly constant, again an indication of good focusing. Test point 33-14 was operated at a feed pressure of 135 mm Hg resulting in a flow rate of 4.65×10^{-7} lb/sec. The resulting I_{sp} and q/m at this point were reduced to 496 sec and 663 C/kg, respectively, indicating that flow rate control has a greater effect on performance than V_s control.

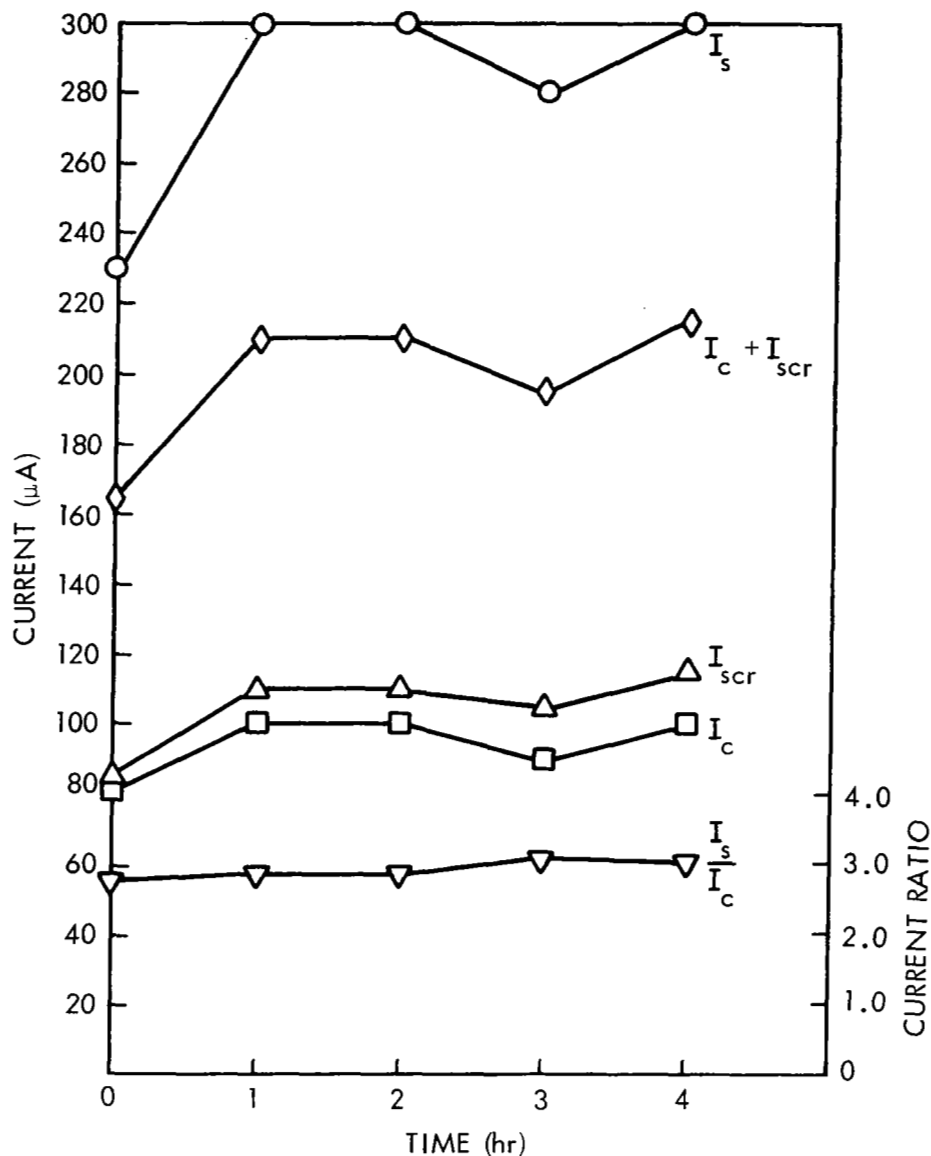


Figure 21—Current versus time for AS-33-1 to 33-5.

At a V_g of 20 kV, a visible glow spray was noticed at the thruster rim. However, examination of data at these points showed that no apparent discontinuity had been introduced into the data. Two conclusions could be drawn from this: The first is that glow spray existed to some extent throughout the test; the second, that glow spray had no effect on total performance. A more complete discussion on this will be presented after test AS-35. Examination of the thruster after the test showed no increase in erosion (Figure 25).

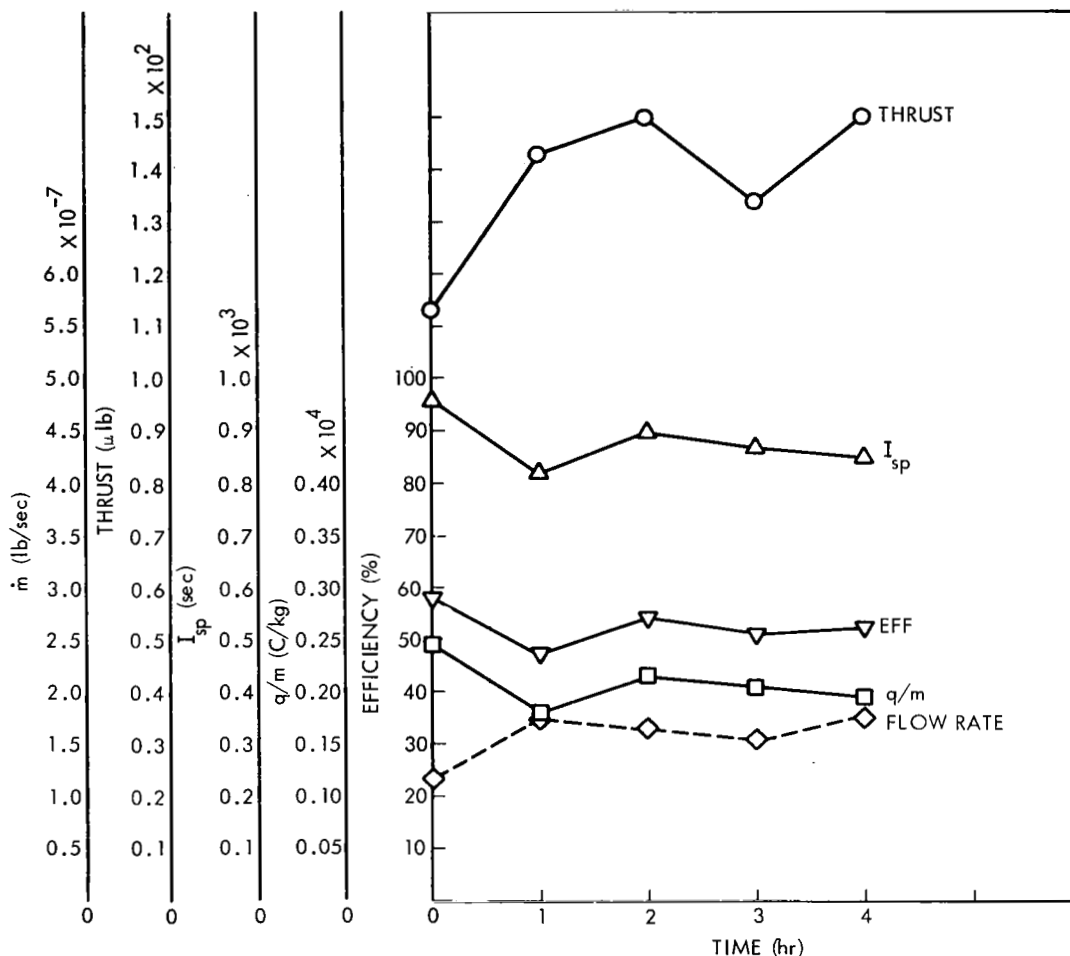


Figure 22--Performance curves for AS-33-1 to 33-5. $V_s = 18$ kV, $V_{ext} = -2$ kV, $V_{scr} = +45$ V, propellant No. 20 was used, and $P_f = 60$ mm Hg.

As a result of the thruster performance in AS-33, AS-35, an extended duration life test of 120 hours, was conducted. The main control function attempted during this test was to maintain V_s so that glow spray would not be sustained. Up through test point 35-6 this was possible. At points 35-7 and 35-9, the thruster had to be idled at about 8 kV for 20 minutes to regain stability and eliminate glow spray. At test point 35-9 and above, glow spray could no longer be eliminated by reducing the voltage which resulted in the remainder of the tests being conducted with glow spray with V_s varying from 15.75 kV to 18 kV. As is shown in Figure 26, performance during the entire test was quite unstable. As seen in Figure 27, the only stable parameter was the ratio of $I_s/(I_c + I_{scr})$, which varied between 1.7 and 2.5.

Test points 35-18 through 35-21 were conducted with increasing feed pressures, which resulted in increased q/m and I_{sp} . This result is contrary to what one would expect and is attributed to the increased glow spray raising the propellant temperature,

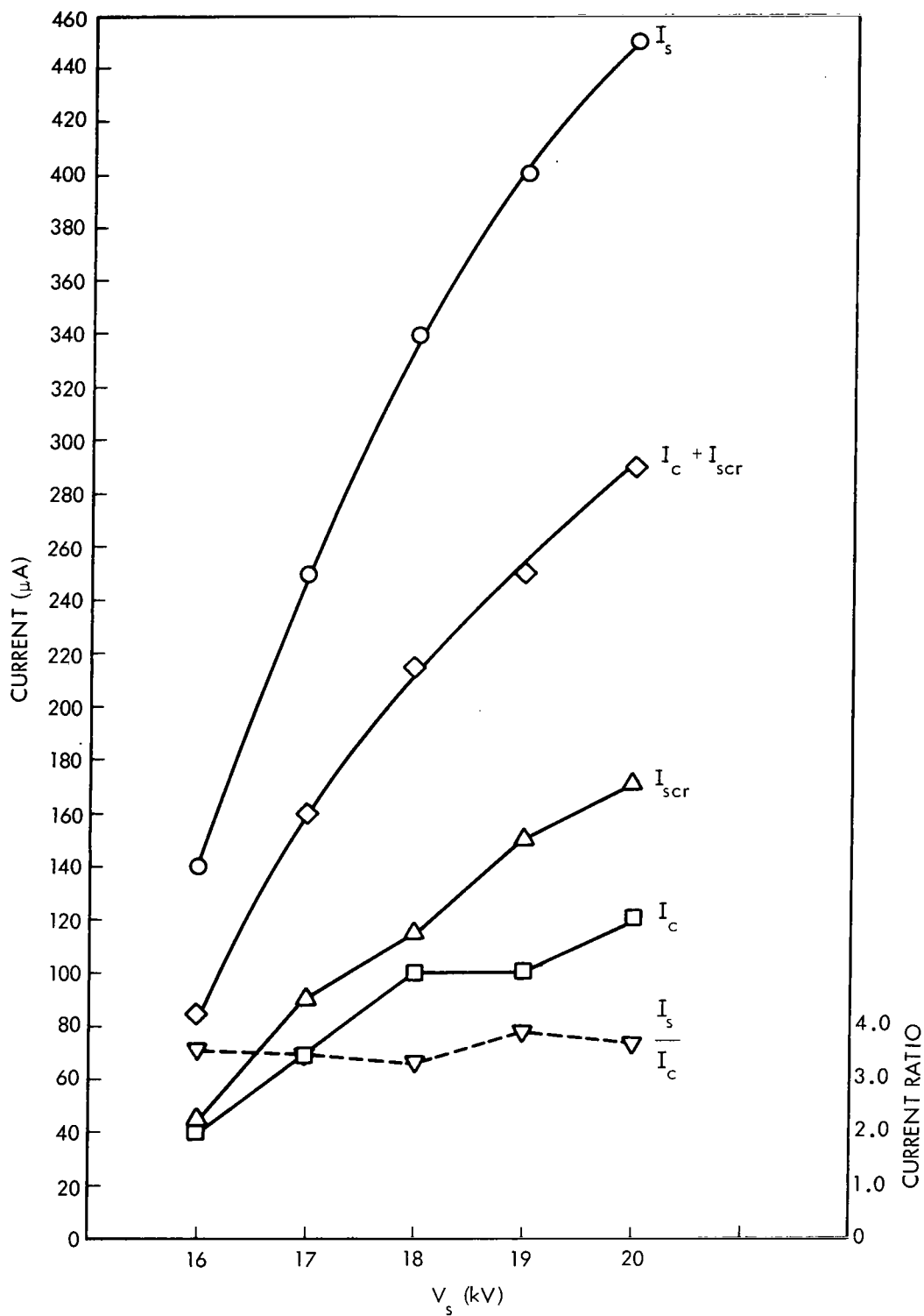


Figure 23—Current versus V_s for AS-33-7 to 33-11.

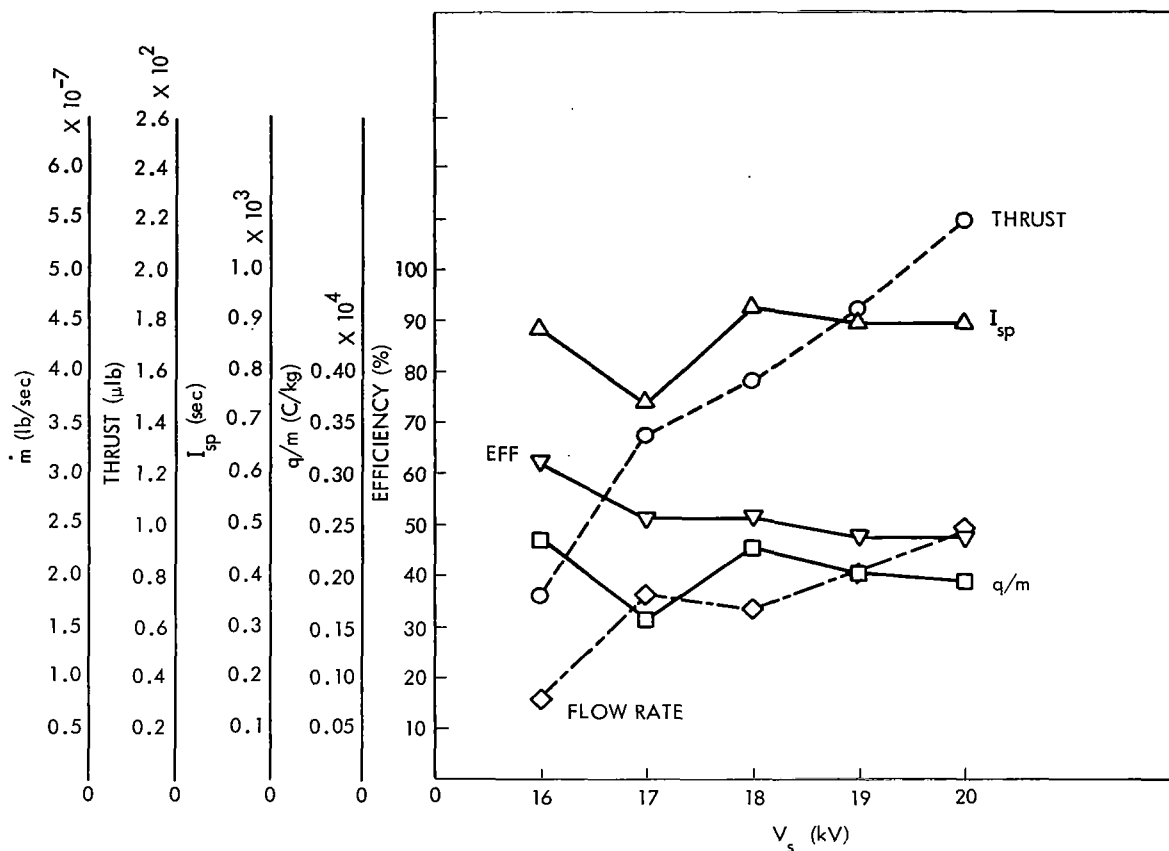


Figure 24—Performance curves for AS-33-7 to 33-11. $V_{ext} = -2$ kV, $V_{scr} = +45$ V, propellant No. 20 was used, and $P_f = 60$ mm Hg.

which caused a larger percentage of propellant to vaporize and not to be reflected in the TOF \dot{m}_c data reduction. Examination of the thruster later showed some erosion of the outer rim (Figure 28), and large deposits were noted on the tapered portion of the outer rim (Figure 29).

A decision, therefore, had to be made with respect to glow-spray operation. Although high but erratic performance was obtained during this mode of operation, the cause and effects of the glow spray were unknown. Several hypotheses are suggested as the cause or possible effects of the glow spray. The first is that the glow spray is the result of electrons' leaving a surface, e.g., collector, screens, or chamber walls, because of particle impact and returning to the thruster, which return causes a self-sustaining action. The second suggests that the glow spray is due to high-velocity particle impact with a local atmosphere caused by propellant vaporization near the thruster. A third hypothesis attributes the glow to interparticle collisions. The fourth hypothesis

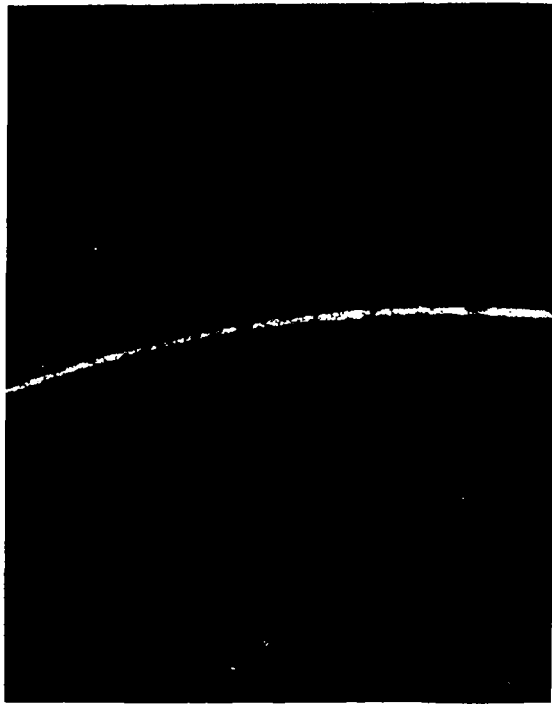


Figure 25--Annular rims after AS-33.

suggests that the glow spray caused excessive local rim heating and lowered the propellant viscosity and resistivity, which then perpetuates the glow phenomena.

After consideration of all four hypotheses, the third was rejected as a possible cause of glow spray that would affect the satisfactory performance of the thruster. If the first, second, or fourth hypotheses were true, however, they would affect the performance of the thruster and cause the recording of erroneous data. For example, if the first hypothesis were true, all the data would be invalid because in the absence of surrounding objects, e.g., in space, there would be no interchange of charges possible. The second and fourth hypotheses would affect stable performance because the temperature rise associated with the glow spray would cause a lowering in propellant viscosity and resistivity and a rise in vapor pressure. All these variations would result in uncontrolled performance variations.

As there was no apparent way to remedy glow spray due to charge interchange and particle collisions, efforts were directed to reducing evaporation of the propellant as a means of eliminating glow spray. It was theorized that if glow spray were due primarily to a high vapor pressure or excessive propellant surface area exposure, a simpler solution was possible.

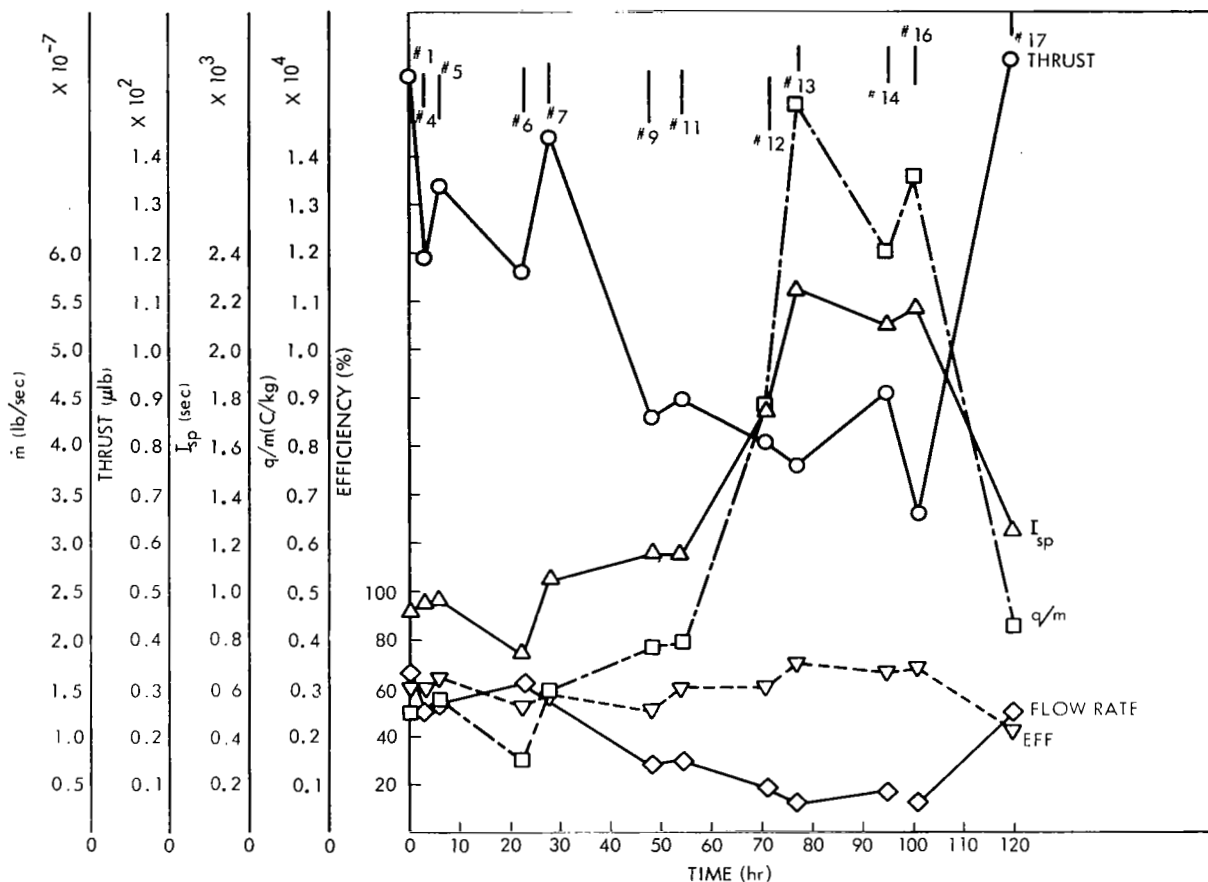


Figure 26—Performance curves for AS-35. $V_s = 15.75$ to 18 kV, $V_{ext} = -2$ kV, $V_{scr} = +45$ V, propellant No. 21 was used, and $P_f = 60$ mm Hg.

Thruster Geometry Variations

The first step taken to eliminate glow spray was to examine the thruster used in AS-35 and measure its annulus gap. From Figure 30 the gap measures 0.006 in., which is approximately 0.004 in. larger than the design gap. This widened gap evidently resulted from successive rim polishings. The effect of this larger annulus area is a larger propellant surface area exposed to the vacuum. Since one factor affecting evaporation is surface area, more propellant was evaporating, which could result in a local atmosphere sufficient to cause glow spray.

To determine the validity of this theory a new thruster was made of 20Cb-3 stainless steel with an annulus of 0.0017 in. (Figure 31). Test AS-37 was conducted using propellant No. 22. A hood was used to darken the chamber, and the rim of the thruster was observed for signs of glow spray. Between values of V_s from 10 to 11 kV, glow spray

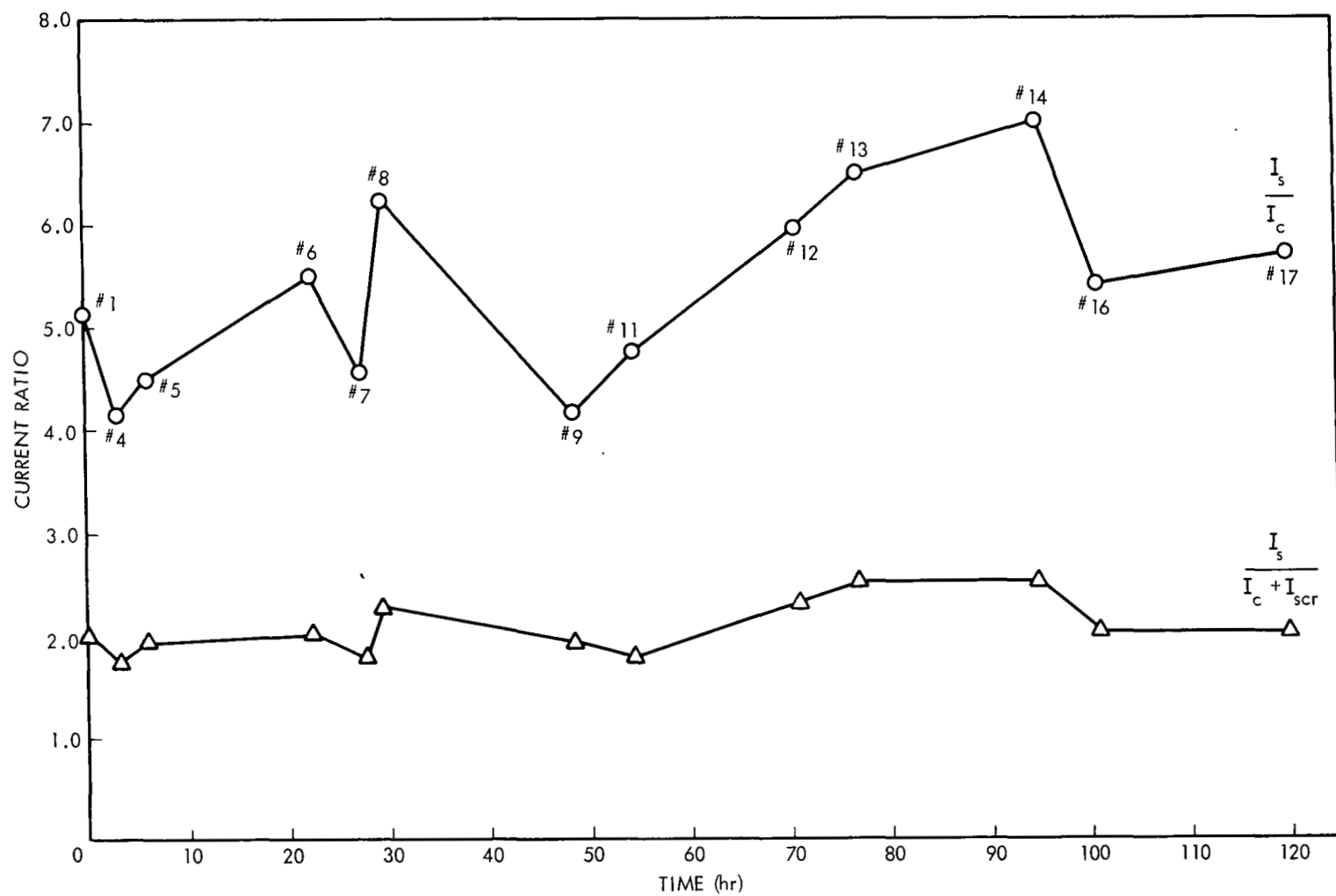


Figure 27—Current versus time for AS-35-1 to 35-17.

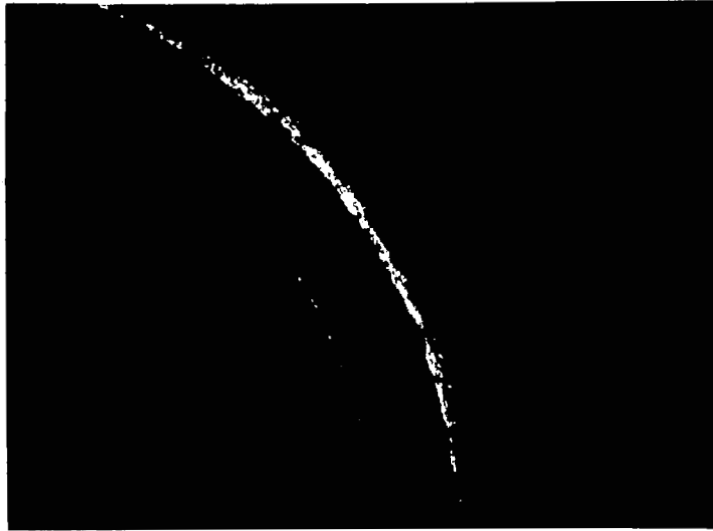


Figure 28—Annular rims after AS-35.

was initiated in one spot on the thruster rim. After 1-1/2 hours V_S could be raised to 13.5 kV without glow spray. After approximately another hour V_S was raised to 15 kV without glow spray. This was the maximum V_S value that could be used without glow spray. At this point a TOF was taken, and the data were presented in Table 3. Performance was very low; however, the flow rate was higher than normal. Slight erosion was noticed when the rim was examined after the test (Figure 32).

An interim test was conducted to determine glow spray visibility in complete darkness and in a lighted room. The thruster V_S was raised to a level at which there was extreme glow spray ($I_S \approx 700 \mu A$). In darkness there was no difficulty in our observing the beam, but in a lighted room, the glow spray was difficult to see. As a result darkroom shades were ordered for the laboratory so that the glow spray could be observed more readily.

Another interim test was conducted to determine effects on glow spray from changes in the radius of the rim. One test was conducted with a 0.0001-in. radius and the other with a 0.0005-in. radius. Glow spray appeared at about 12 kV in both cases. During this testing it was noticed, as in other tests, that the feedline inside the chamber acquired a dark coating and was warm. Because this line is at V_S , it is possible that electrons bombarded it during the test which caused heating of the line and propellant and affected flow rates and performance.

A thermometer was inserted in the feedline to determine its temperature rise, and test AS-42 was run. Four test points were taken under non-glow-spray conditions. Performance was higher than AS-37, but still too low to be acceptable. After 105 minutes the feedline temperature had risen 27 Fahrenheit degrees. A screen shield was made and placed around the feedline and biased at -2 kV.



Figure 29—Depcsit on outer rim after AS-35.

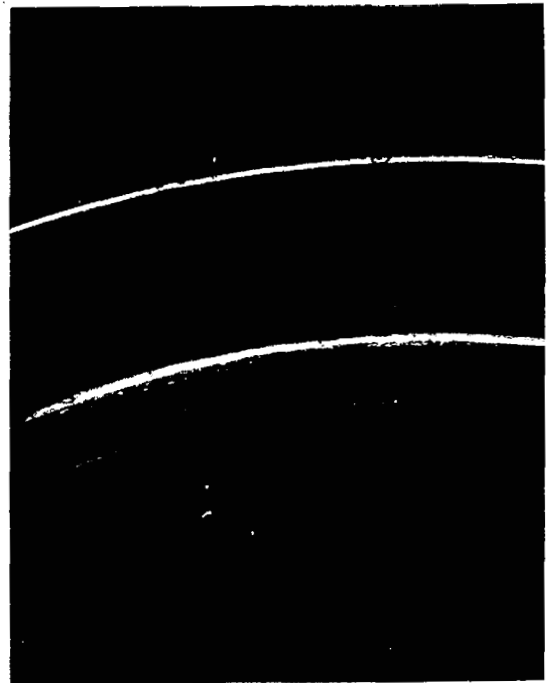


Figure 30—The 0.006-in annulus gap.

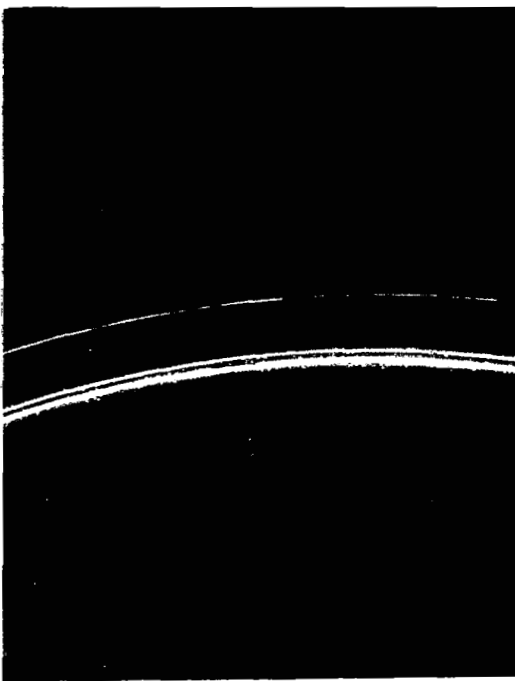


Figure 31—The 0.0017-in. annulus gap.

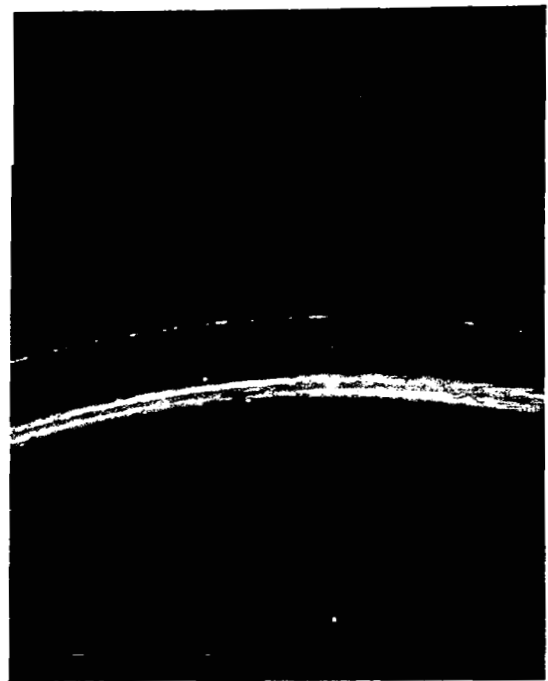


Figure 32—Annular rims after AS-37.

Test AS-43 was conducted to determine the effect of this wire shield. After 90 minutes of operation at a V_S of 15 kV, there was no rise in feedline temperature, which verified the electron bombardment theory; however, another important observation was made. I_S and I_C were, respectively, 100 μ A and 20 μ A lower for test AS-43 than for test AS-42, which was conducted under conditions identical with AS-43 except for the negative wire shield. This indicates that in previous tests a large percentage of I_S was due to the electron impingement on the feedline, which caused a fictitiously high current. Examination of the thruster after the test indicated no erosion. All subsequent tests were run with the wire shield.

As a result of tests AS-37 through AS-43, it was shown that acceptable performance without glow spray could not be obtained through a reduction in exposed propellant surface area in the annulus, a variation in rim radii, and the elimination of propellant temperature rise due to feedline bombardment by electrons.

Propellant Investigation

The second step in the investigation to eliminate glow spray was to develop new propellant combinations with lower vapor pressures than NaI-glycerol. This measure was based on the same assumption that glow spray is caused by excessive vapor accumulating in the vicinity of the thruster rims.

The first step taken was to investigate a number of low-vapor-pressure solvents and solutes.

Table 4, in addition to the standard glycerol solutions, contains the solute-solvent combinations that become conductive. Only solvents with lower vapor pressures than glycerol were considered in this investigation. Many solvents and solutes were tried which were not suitable for various reasons. Among the solvents that would not dissolve solutes or become conductive were the silicone oils, Santovac-5 oil, Convoil 20 oil, Octoil, and Duo Seal oil. A solvent that became slightly conductive but not enough to consider for a test was 65 Quanta Lube.

The solutes used for doping purposes were sodium tetraethylenediamine tetraacetate, sodium acetate, benzyldimethylphenylammonium chloride, phenylhydrazine hydrochloride, Dibutyldichlorotin, lithium chloride, ammonium chloride, sodium bromide, sodium iodide, cesium carbonate, cesium chloride, cesium fluoride, sodium chloride, sulfuric acid, polyphosphoric acid, acetic acid, tetraethyl ammonium chloride, tetraphenyl tin, di-*n*-butyl tin diacetate, sodium hydroxide, sodium nitrate, nitric acid, zinc chloride, laurylisoquinolinium bromide (No. 503), diisobutylphenoxyethoxyethyl dimethylbenzyl ammonium chloride (No. 488), and octadecyltrimethyl ammonium chloride (No. 474).

Several problems were encountered with all combinations not listed in Table 4. These included insolubilities, chemical reactions, increased viscosity, high resistivities, reverse solubilities, and precipitation of the solutes. Figures 33 through 36 are curves depicting the variations of resistivities of various solutes dissolved in the three basic solvents used (Carbowax-400; glycerol; and 1, 2, 6-hexanetriol).

Table 4 — Propellant combinations.

Propellant solutions (mixed and degassed under vacuum)			Vapor pressure of solvent (mm Hg, °F)	Resistivity (Ω -cm, °F)	Comments
No.	Solute	Solvent			
1.	5 gm NaI	100 ml Carbowax-400 (Polyethylene glycol)	1.5×10^{-7} , 122°F	6600, 78°F	-
2.	10 gm NaI	100 ml Carbowax-400 (Polyethylene glycol)	1.5×10^{-7} , 122°F	4900, 77°F	-
3.	6 gm NaNO ₃	100 ml Carbowax-400 (Polyethylene glycol)	1.5×10^{-7} , 122°F	4600, 77°F	-
4.	5.7 gm LiCl	100 ml Carbowax-400 (Polyethylene glycol)	1.5×10^{-7} , 122°F	11 500, 77°F	-
5.	14.3 gm NaBr	100 ml Carbowax-400 (Polyethylene glycol)	1.5×10^{-7} , 122°F	7400, 77°F	Reverse solubility occurred
6.	5 gm NaOH	100 ml Carbowax-400 (Polyethylene glycol)	1.5×10^{-7} , 122°F	47 000, 77°F	-
7.	3 gm NH ₄ Cl	100 ml Carbowax-400 (Polyethylene glycol)	1.5×10^{-7} , 122°F	6050, 77°F	Reverse solubility occurred
8.	11 gm CsCl	100 ml Carbowax-400 (Polyethylene glycol)	1.5×10^{-7} , 122°F	4600, 77°F	Reverse solubility occurred
9.	4.6 gm Phenylhydrazine hydrochloride	100 ml Carbowax-400 (Polyethylene glycol)	1.5×10^{-7} , 122°F	18 600, 77°F	Reverse solubility occurred
10.	462 drops of No. 503	100 ml Carbowax-400 (Polyethylene glycol)	1.5×10^{-7} , 122°F	41 000, 77°F	-
11.	460 drops of No. 488	100 ml Carbowax-400 (Polyethylene glycol)	1.5×10^{-7} , 122°F	24 000, 77°F	-
12.	7.5 gm of No. 474	100 ml Carbowax-400 (Polyethylene glycol)	1.5×10^{-7} , 122°F	17 500, 77°F	-
13.	4 gm NaI-No. 488	100 ml Carbowax-400 (Polyethylene glycol)	1.5×10^{-7} , 122°F	8000, 77°F	-
14.	9 gm NaI	100 ml 65 Quanta Lube	$< 10^{-8}$	185 000, 77°F	-
15.	33 gm Dibutyldichlorotin	100 ml 1,2,6-hexanetriol	-	280 000, 77°F	Very viscous
16.	30 gm NaI	100 ml 1,2,6-hexanetriol	-	18 200, 77°F	-
17.	5 gm NH ₄ Cl	100 ml 1,2,6-hexanetriol	-	14 500, 77°F	Precipitated out
18.	35 gm NaI	117 ml glycerol	4×10^{-3} , 122°F	4650, 77°F	-
19.	37 gm NaI	120 ml glycerol	4×10^{-3} , 122°F	3850, 77.5°F	-
20.	30 gm NaI	100 ml glycerol	4×10^{-3} , 122°F	4500, 77°F	-
21.	43 gm NaI	125 ml glycerol	4×10^{-3} , 122°F	4000, 79°F	-
22.	35 gm NaI	100 ml glycerol	4×10^{-3} , 122°F	4300, 76.5°F	-
23.	20 gm NaI	100 ml glycerol	4×10^{-3} , 122°F	5750, 77°F	-

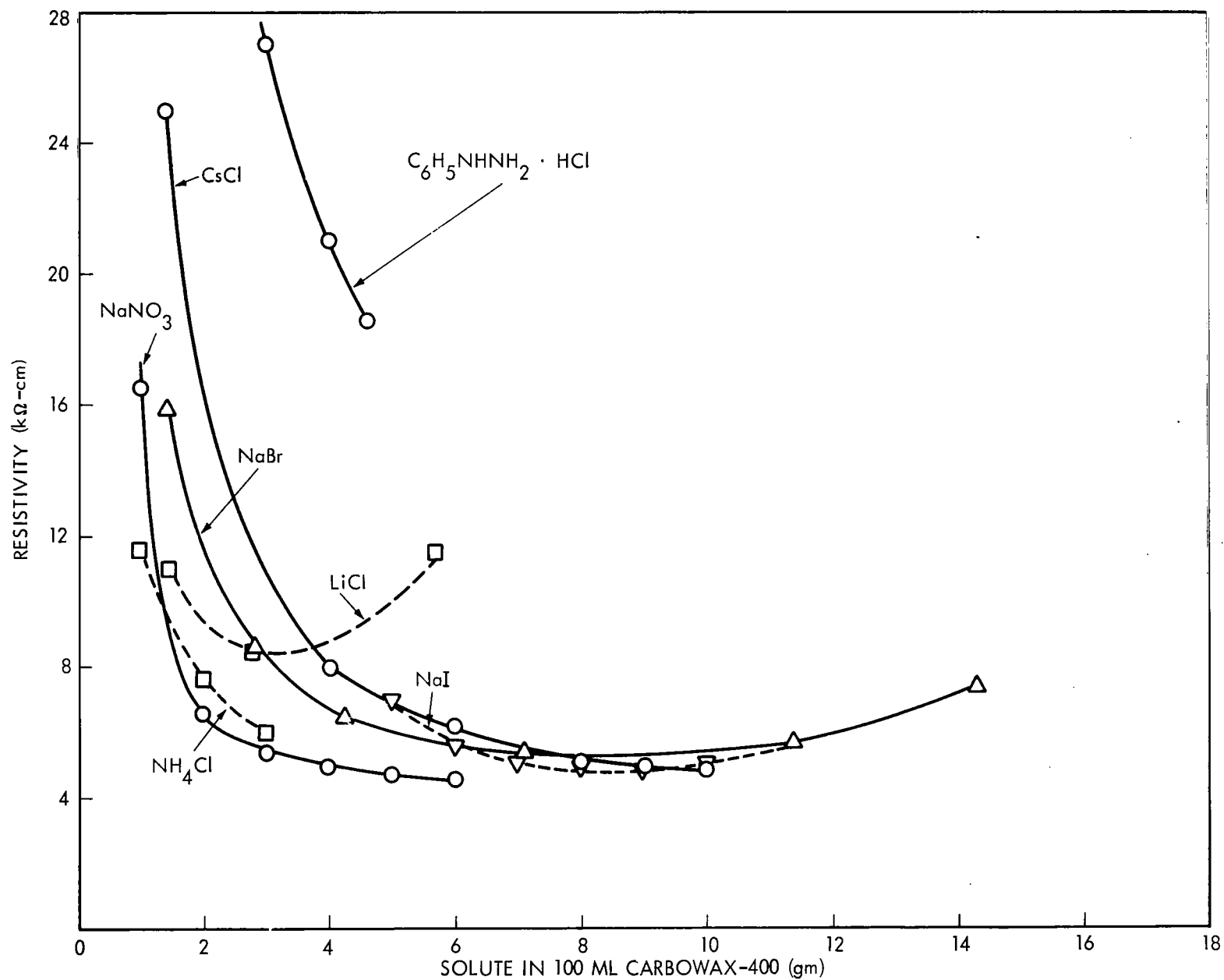


Figure 33—Solution resistivity of solutes dissolved in 100 ml of Carbowax-400.

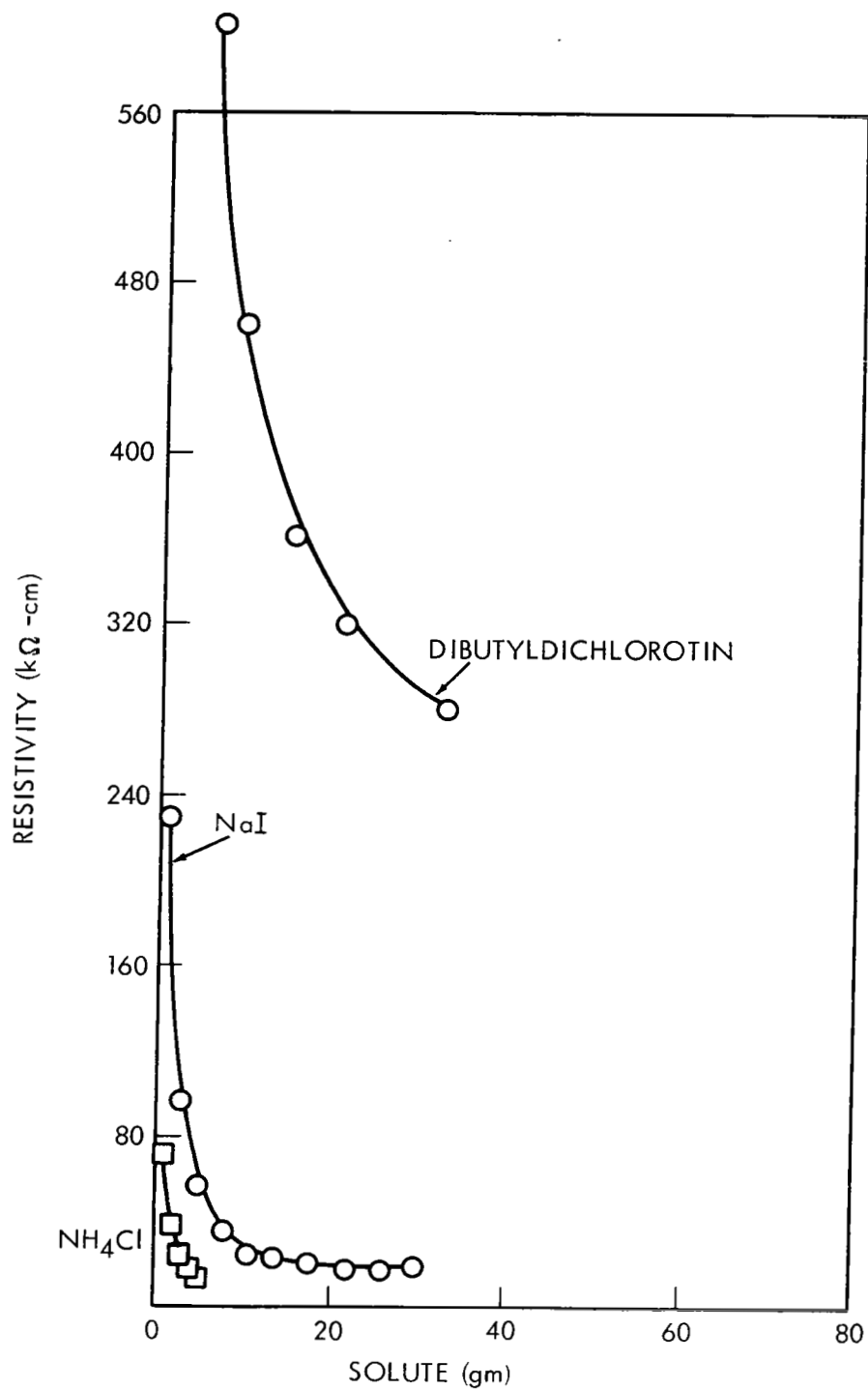


Figure 34—Solution resistivity of solutes dissolved in 100 ml of 1, 2, 6-hexanetriol.

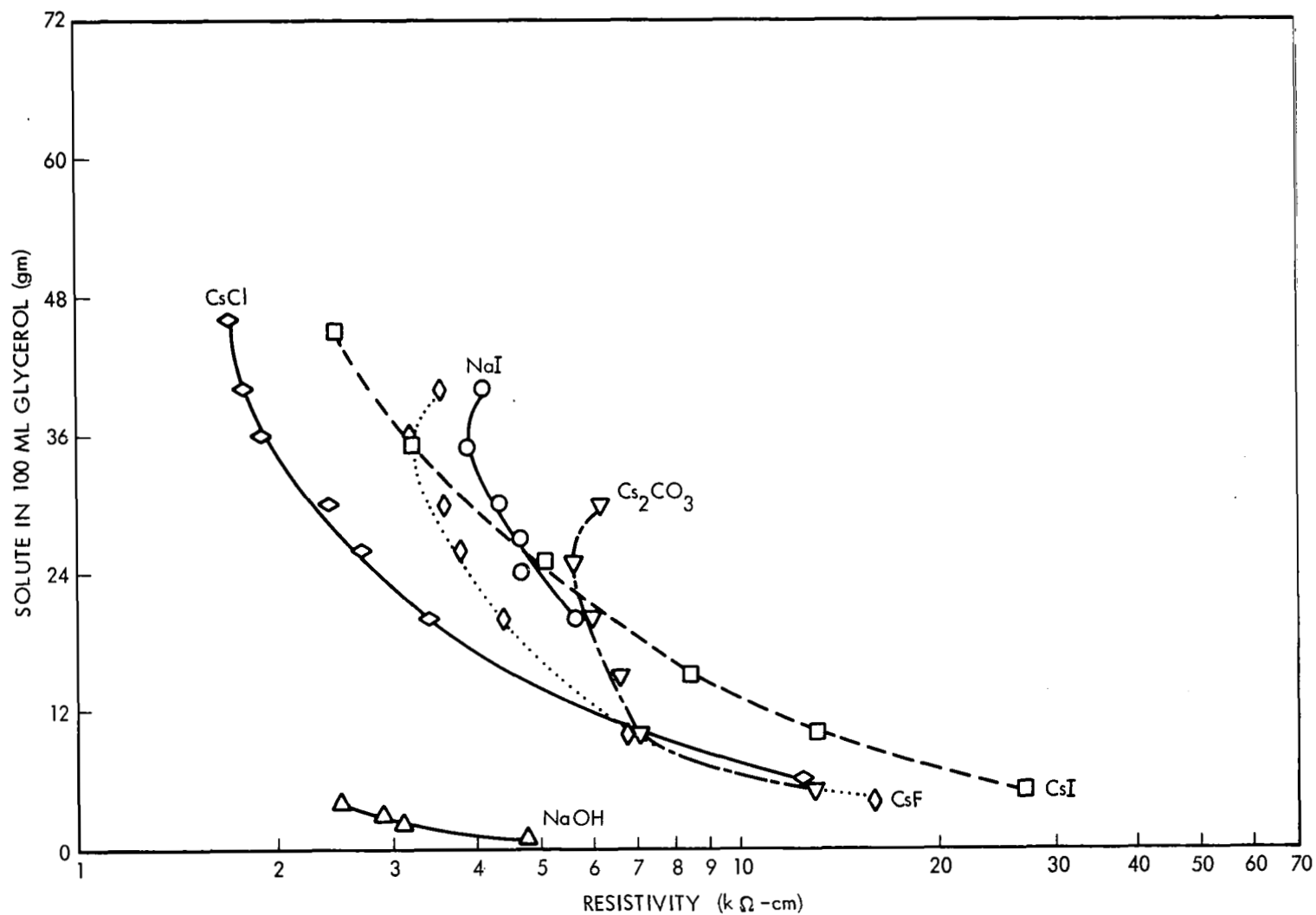


Figure 35—Solution resistivity of various solutes dissolved in 100 ml of glycerol.

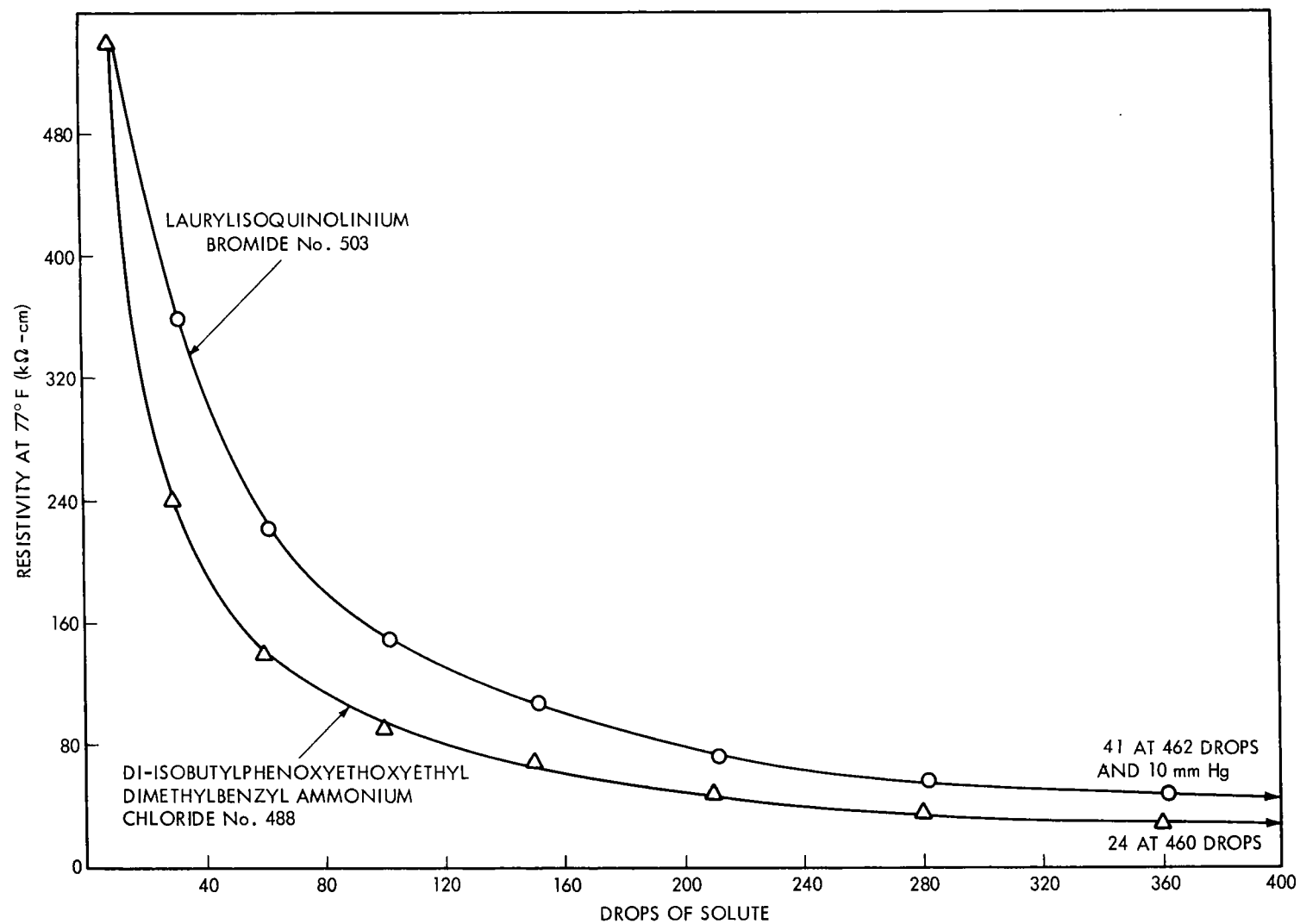


Figure 36 – Solution resistivity of liquid solutes in Carbowax-400.

AS-45 was the first test conducted with a new propellant, propellant No. 1, and with a flow control orifice. At a V_s of 19 kV there was no glow spray; however, performance was far from acceptable. The flow rate was higher than with the glycerol solutions, which obviously contributed to the low performance. The TOF trace is shown in Figure 37.

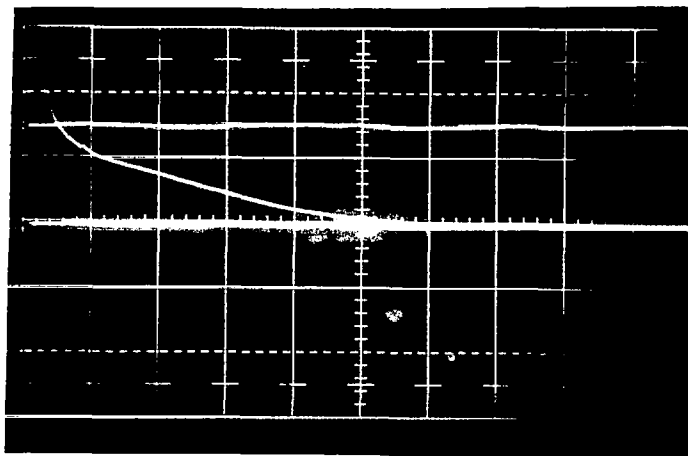


Figure 37—TOF trace of AS-45-1. $V_s = 19$ kV, $I_s = 75$ μ A, $i = 5$ μ A/cm, and the sweep was 50 μ sec/cm.

Test AS-46 was conducted with propellant No. 2. Propellant No. 2 is propellant No. 1 doped with additional solute for a lower resistivity. The orifice was removed, and a clamp was used on the feedline as a flow restrictor. Test points 46-1, 46-2, 46-4, and 46-5 were taken. Test points 46-1, 46-2, and 46-4 showed slight improvements in performance over AS-45. The feedline was clamped tightly to stop all flow to determine the effect of reduced flow. After 1-3/4 hours glow spray commenced. At this time test point 46-5 was taken with a resultant I_{sp} of 1168 sec and an ACMR of 5738 C/kg. The flow rate was down to 0.885×10^{-7} lb/sec from a high of 7.75×10^{-7} lb/sec. It appears that performance was improving as \dot{m}_t was decreasing until a point was reached at which glow spray began. Again, because of the limited understanding of the exact nature of glow spray, a precise explanation is not possible. However, in this instance as \dot{m}_t decreased, glow spray could have been a result of the increasingly higher energy particles releasing more electrons from the collector and other impact surfaces to bombard the thruster rim and fluid surface. This bombardment would result in higher propellant temperature and vapor pressure.

Upon shutdown of this test, the thruster was very hot with an estimated temperature of 150°F. A quick check showed the resistivity of this propellant at 155°F to be 700 Ω -cm. The vapor pressure of the solvent (Carbowax-400) at this temperature is 3×10^{-3} mm Hg. Both of these could certainly have been the cause of the glow spray.

Examination of the thruster after the test showed erosion on both rims (Figure 38). The TOF traces are shown in Figures 39 through 42.

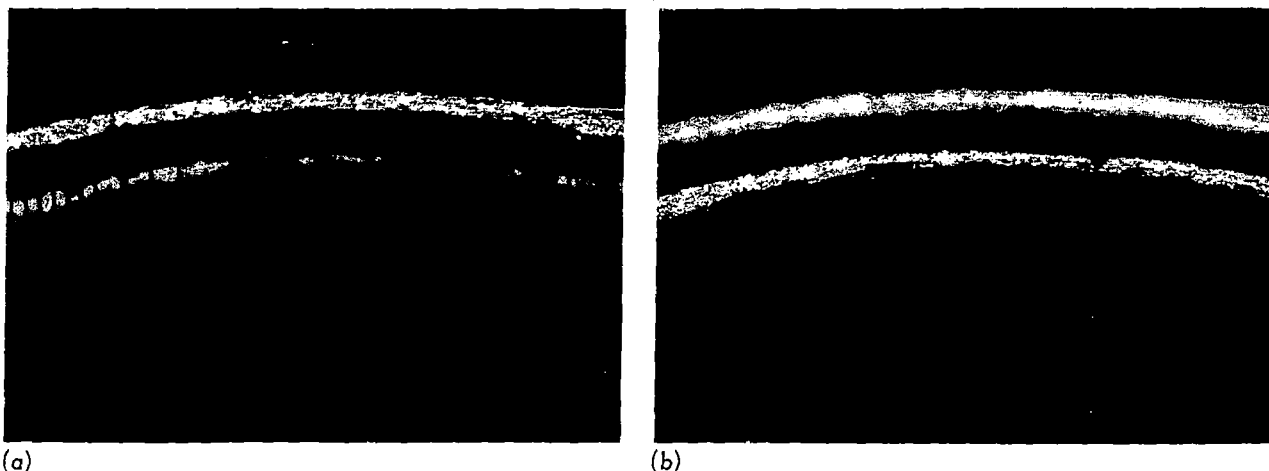


Figure 38—Annular rims after AS-46, (a) outer rim in focus, and (b) inner rim in focus.

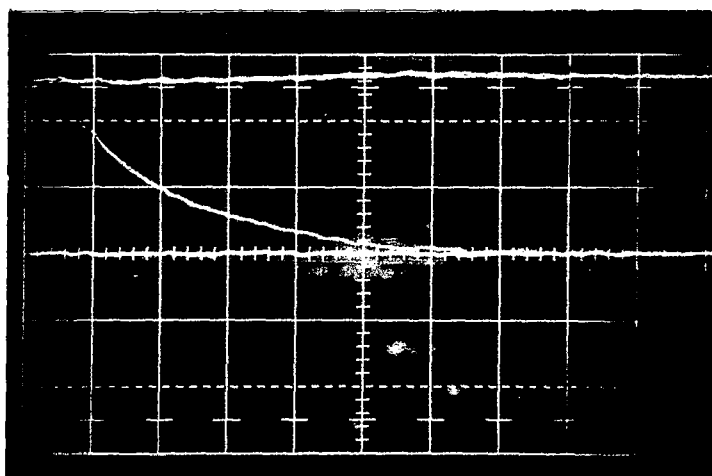


Figure 39—TOF trace of AS-46-1. $V_s = 19.25$ kV, $I_s = 100$ μ A, $i = 10$ μ A/cm, and the sweep was 20 μ sec/cm.

Test AS-47 was conducted using propellant No. 3 to continue investigation of the effect of the propellant. V_s was raised to 20 kV with no glow spray. Performance was again poor. The test was terminated after 1-1/2 hours. Examination of the thruster after the test showed rim erosion (Figure 43). The erosion is difficult to explain because, unlike AS-46, there was no glow spray and the thruster was not warm. The TOF trace is shown in Figure 44.

AS-48 was the next test conducted and used propellant No. 5. V_s had to be set at 21.5 kV to obtain stable performance. As shown in Table 3, performance was still low. After 1 hour, glow spray commenced and the test was terminated. As in AS-46, the thruster was very hot. Examination of the thruster after the test showed severe rim erosion (Figure 45). The TOF trace is shown in Figure 11.

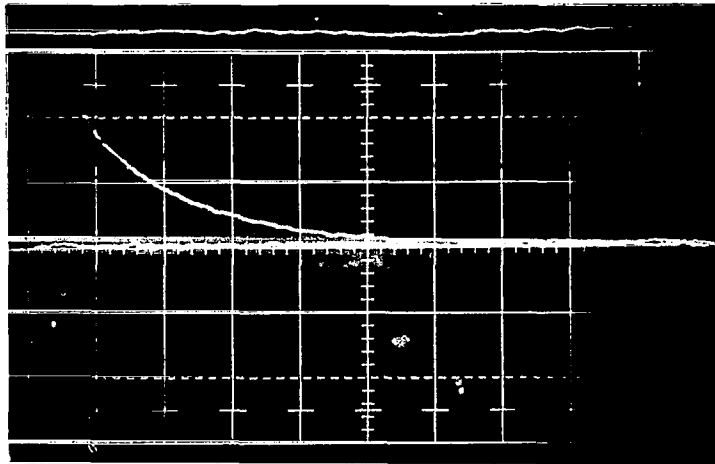


Figure 40—TOF trace of AS-46-2. $V_s = 20.25$ kV, $I_s = 100$ μ A, $i = 10$ μ A/cm, and the sweep was 20 μ sec/cm.

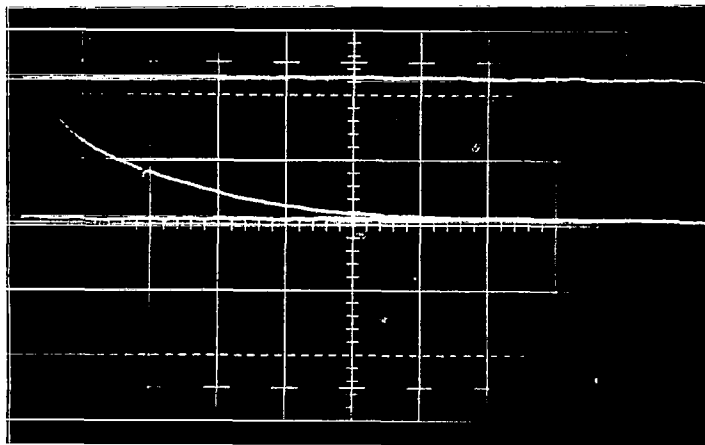


Figure 41—TOF trace of AS-46-4. $V_s = 18.5$ kV, $I_s = 200$ μ A, $i = 20$ μ A/cm, and the sweep was 20 μ sec/cm.

Testing was halted at this point so that the problem of thruster erosion could be investigated. Up through test AS-35 there had been no erosion as severe as that which occurred in later tests. Tests conducted after AS-35 were done with the new thruster. It was thought possible that the thruster was not 20Cb-3 stainless steel but rather a less corrosive resistant steel. An emission spectrograph analysis was run on a sample bar of 20Cb-3 stainless steel, the old annular thruster, and the new one. The results were identical, which proved that the three items were of the same metal (i.e., 20Cb-3 stainless steel). Because the material was the proper one, the next possible explanation for the erosion would be improper heat treatment of the base metal. To determine if this

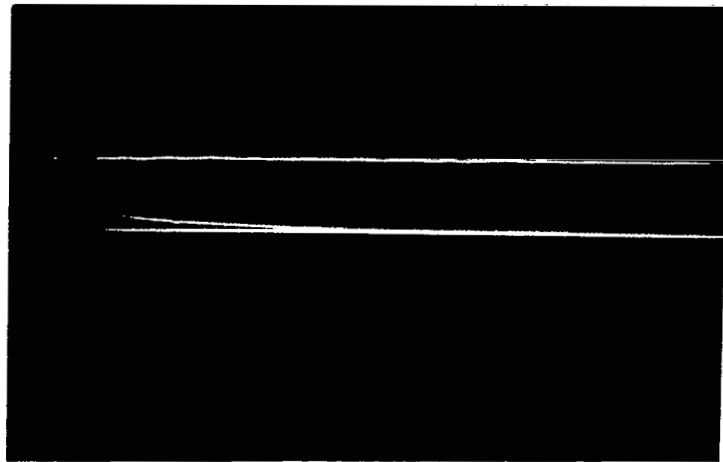


Figure 42—TOF trace of AS-46-5. $V_s = 18$ kV, $I_s = 230$ μ A, $i = 50$ μ A/cm, and the sweep was 10 μ sec/cm.



Figure 43—Annular rims after AS-47.

were the case, a destructive test would have had to be run on the sample. A segment of metal would have had to be removed and then subjected to a polishing-etching procedure. Since this would have meant the destruction of the thruster, this analysis could not be considered.

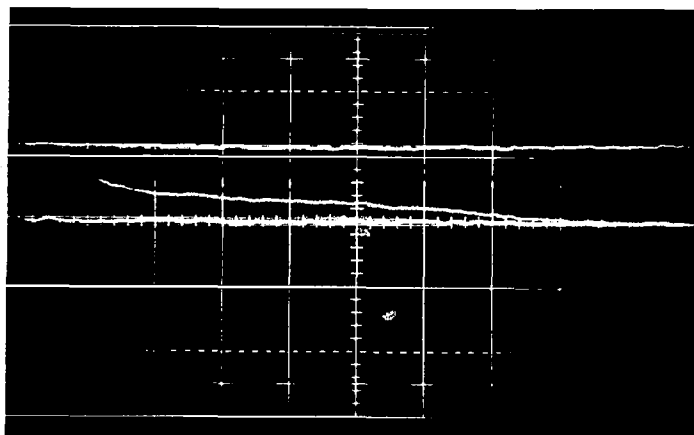
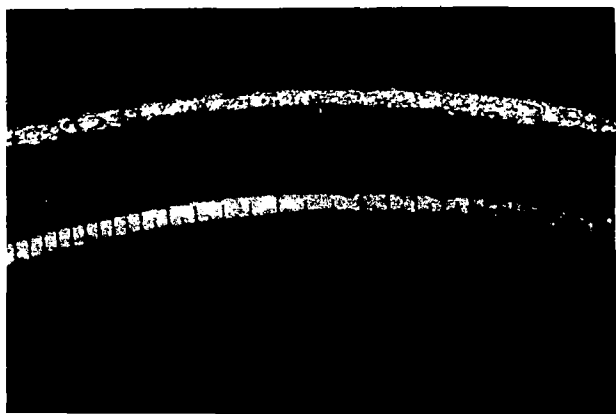
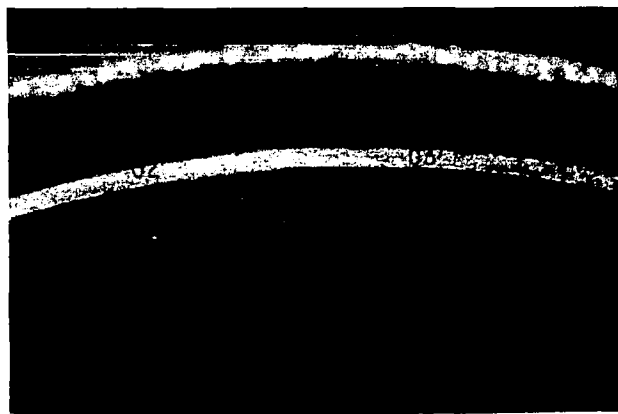


Figure 44—TOF trace of AS-47-4. $V_s = 20$ kV, $I_s = 75$ μ A, $i = 10$ μ A/cm, and the sweep was 20 μ sec/cm.



(a)



(b)

Figure 45—Annular rims after AS-48, (a) outer rim in focus, and (b) inner rim in focus.

It was decided to plate all the new thruster rims with platinum to prevent further erosion so that the program could continue without further delay.

Test AS-49 was the first with these platinum-plated thrusters and used propellant No. 8. Above a V_s of 15 kV, a bluish-purple glow spray, unlike the typical bright-orange glow spray when NaI is used as a solute, emanated from the rims. At a V_s of 20 kV there was no discernible I_s . After 1 hour the test was terminated. Examination of the thruster after the test showed no erosion (Figure 46).

Test AS-50 was the first evaluation of propellant No. 11, a surfactant used as the dopant. Performance was extremely poor, which may have been due in part to the high flow rate. The TOF trace is shown in Figure 47. Examination after the test showed no erosion (Figure 48).

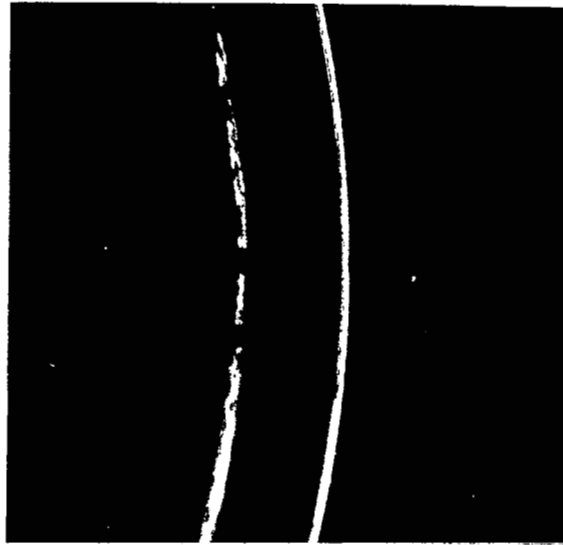


Figure 46—Annular rims after AS-49.

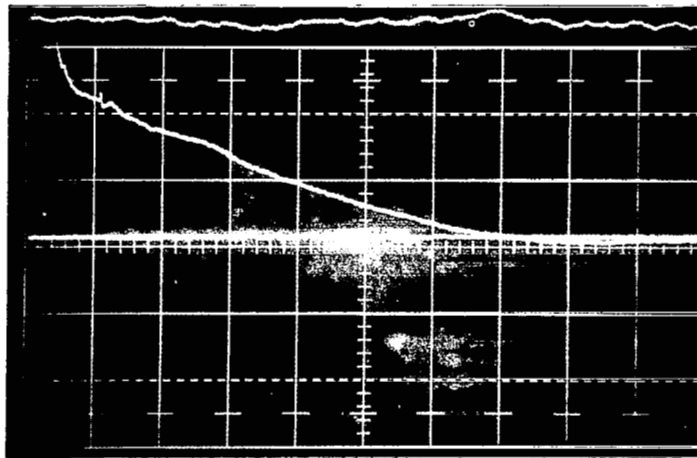


Figure 47—TOF trace of AS-50-1. $V_s = 19.5$ kV, $I_s = 50$ μ A, $i = 1$ μ A/cm, and the sweep was 50 μ sec/cm.

Test AS-51 was the first evaluation of a three-part propellant solution, propellant No. 13. The results were very disappointing. At a value of 20 kV of V_s , there was no discernable I_s and less than 1 μ A of I_c . The test was terminated after 1 hour. Examination of the thruster after the test showed no erosion (Figure 49).

Test AS-52 was conducted with propellant No. 9. Performance was low, and at the maximum V_s value of 22 kV, no glow spray was noticed. The TOF trace is shown in Figure 50. Examination of the thruster after the test showed slight roughening of the rim; however, it did not warrant repolishing for the next test (Figure 51).

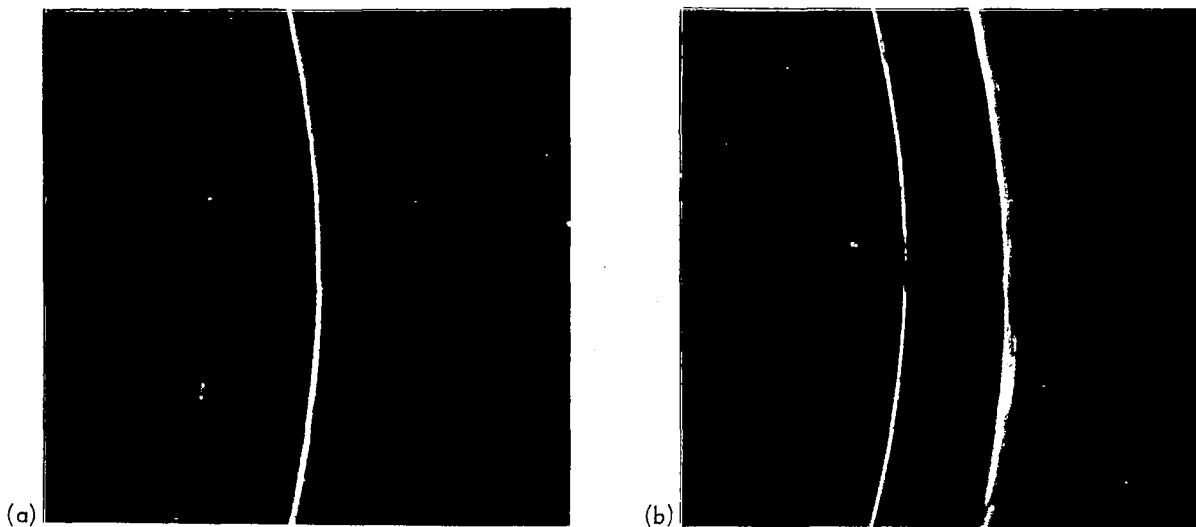


Figure 48—Annular rims after AS-50, (a) outer rim in focus, and (b) inner rim in focus.

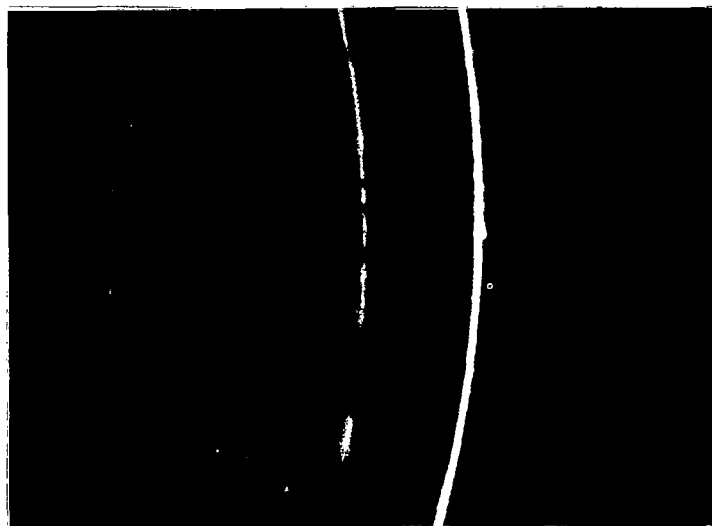


Figure 49—Annular rims after AS-51.

Test AS-53 was run with propellant No. 16. Results were very encouraging because acceptable performance was obtained at a low V_3 without glow spray. The TOF trace is shown in Figure 52. Examination of the rim after the test showed a slight increase in roughening (Figure 53) but not enough to warrant repolishing.

Although this test had the highest performance of the non-glow-spray tests, it also had the second highest resistivity ($18\,200\ \Omega\text{-cm}$, 77°F). In all previous colloid testing, it had been accepted that performance was an inverse function of resistivity; however,

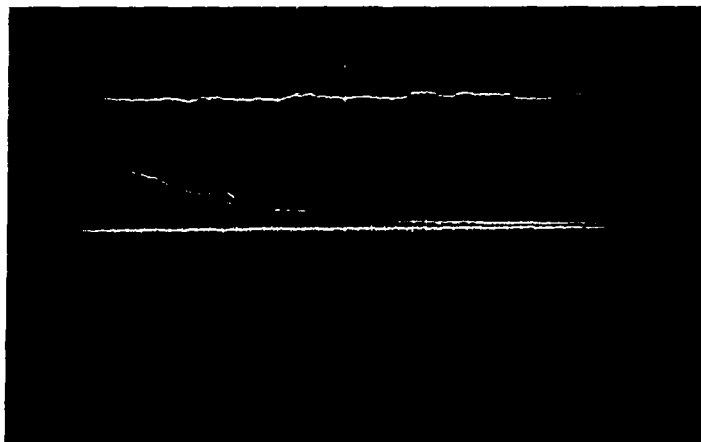
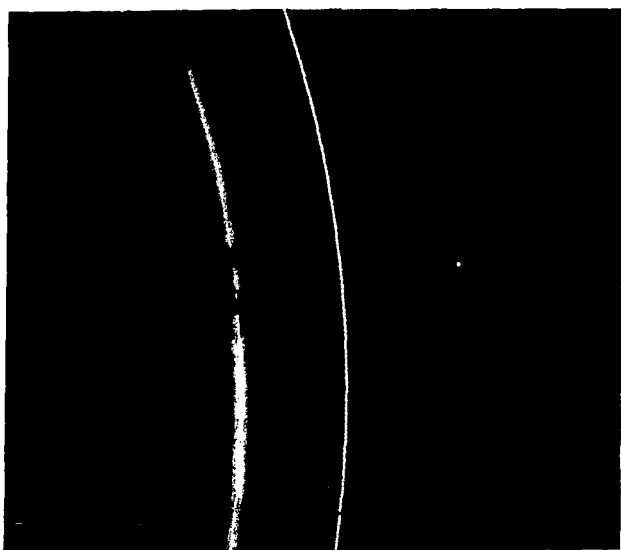
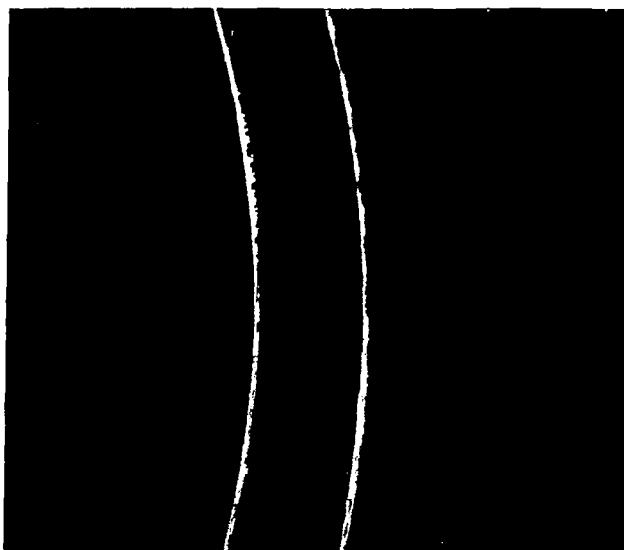


Figure 50—TOF trace of AS-52-1. $V_s = 22 \text{ kV}$, $I_s = 30 \text{ } \mu\text{A}$,
 $i = 1 \text{ } \mu\text{A/cm}$, and the sweep was $50 \text{ } \mu\text{sec/cm}$.



(a)



(b)

Figure 51—Annular rims (a) before and (b) after AS-52.

the above results showed that this was not necessarily true. Also it was noticed that the value of \dot{m}_t was one of the lowest for the non-glow-spray tests and was the lowest for those tests involving NaI-glycerol as the propellant. Before pursuing investigation of the NaI-1,2,6-hexanetriol propellant, it was decided to reinvestigate NaI-glycerol at lower flow rates with a flow control orifice.

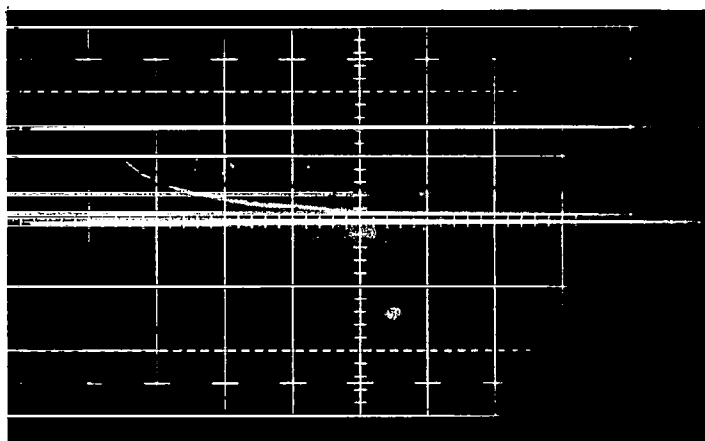


Figure 52—TOF trace of AS-53-5. $V_s = 15.25$ kV, $I_s = 50$ μ A, $i = 5$ μ A/cm, and the sweep was 10 μ sec/cm.

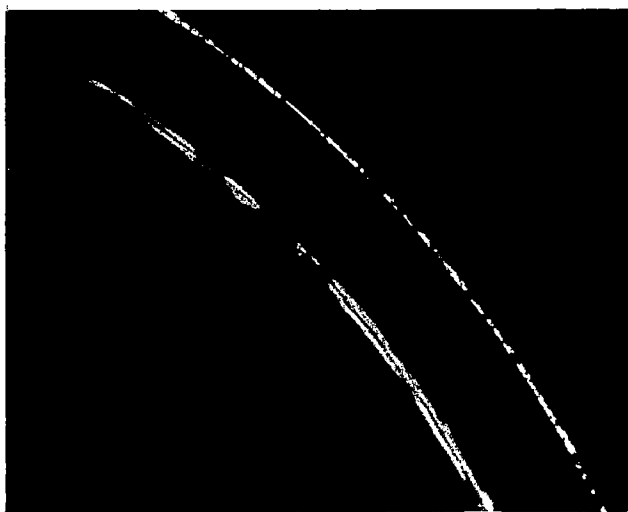


Figure 53—Annular rims after AS-53.

Flow Control Tests

The third step taken to eliminate glow spray was to minimize propellant vaporization due to propellant residence time in the thruster annulus. Calibrated orifices were used to control the flow rate considerably below the level that was originally governed by the flow annulus at 1.67×10^{-7} lb/sec. Test AS-54 was conducted with propellant No. 23 and a flow control orifice calibrated for a flow rate of 0.5×10^{-7} lb/sec.

Three test points were taken, two without glow spray and one with glow spray. Test point 54-2 was without glow spray; point 54-3, with glow spray. Both are recorded in Table 3. As can be seen, performance was low and the flow rates varied from 3.6 to 8.3 times the calibrated orifice value. After 4 hours the test was terminated. After shut-down, the thruster was warm to the touch. This heating effect could be the explanation for the higher flow rates experienced. Examination of the thruster after the test showed no increase in erosion (Figure 54). The TOF traces for test points 54-2 and 54-3 are shown in Figures 55 and 56.

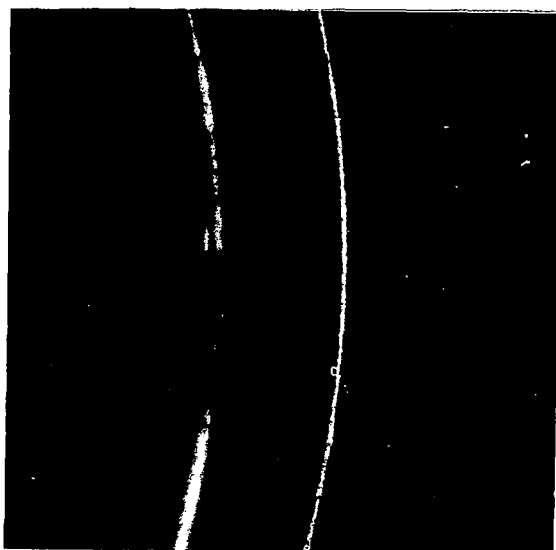


Figure 54—Annular rims after AS-54.

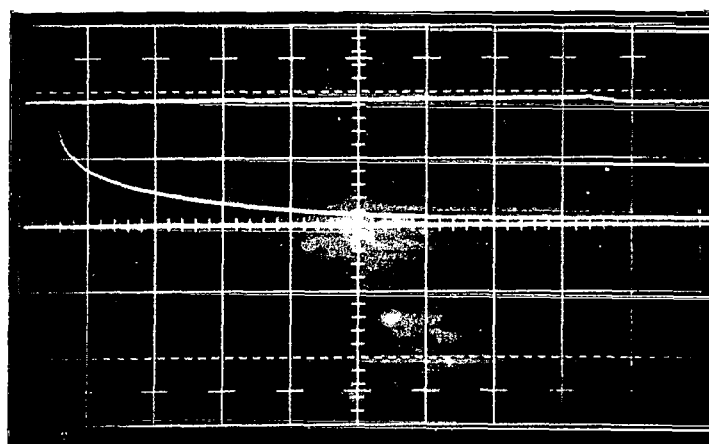


Figure 55—TOF trace of AS-54-2. $V_s = 19.75$ kV, $I_s = 50$ μ A, $i = 5$ μ A/cm, and the sweep was 20 μ sec/cm.

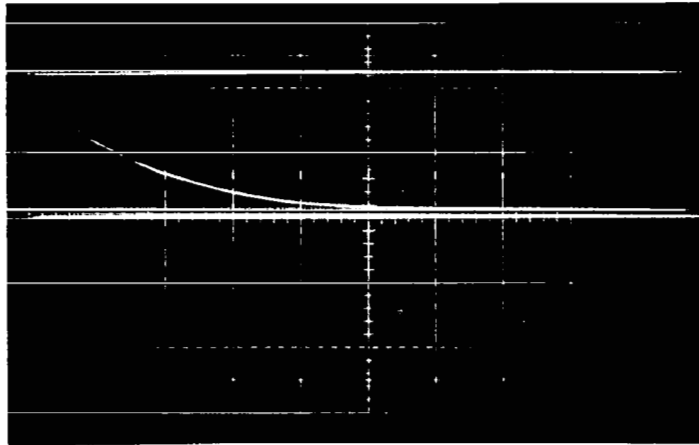


Figure 56-TOF trace of AS-54-3. $V_s = 18.25$ kV, $I_s = 125$ μ A, $i = 10$ μ A/cm, and the sweep was 20 μ sec/cm.

A smaller orifice was used with propellant No. 23 to produce a calibrated flow of 0.03×10^{-7} lb/sec in an attempt to further decrease \dot{m}_t . Test AS-55 was conducted with no glow spray during the three test points taken. Points 55-1 and 55-3 are reported in Table 3. The results were again low, with the flow rates varying from 21 to 28 times the calibrated flow. From this and past data it appears that the desired low flow rates will not be obtained until the propellant temperature can be regulated. A major factor in the problem is the heating of the thruster and propellant by the apparent back bombardment of the thruster rim by electrons with the subsequent glow spray creating additional heating.

Unfortunately the effort required to produce a stable flow rate was of such magnitude as to preclude any sophisticated attempt at the solution of this problem during this program. It would have required substantial redesign and testing to minimize electron bombardment and a system by which constant propellant temperature could be maintained.

As an alternative it was decided to forgo testing of this annular thruster and to test the larger annular thruster (Figure 4), where flow rates proportional to the rim circumference could be more easily obtained. That is, with the small thruster the low flow rate of 0.03×10^{-7} lb/sec was chosen arbitrarily. If it is assumed that firing takes place on the outer rim only (which is reasonable based on typical erosion patterns), the flow per unit length of rim is 0.113×10^{-7} lb/sec per inch of circumference. With this flow rate parameter, the larger thruster would have a total flow rate of 0.27×10^{-7} lb/sec. With this approach, the propellant should remain at the rim for a shorter period of time, and the mechanical problems that arose in attempting to achieve and maintain the very low flow rates associated with the previous thruster should not be incurred.

As mentioned in the test section of this report, several changes were made in the test apparatus before testing the large thruster. A stainless steel collector completely surrounded by a grounded screen (Figure 14) replaced the melamine one, and a thyratron zapper circuit replaced the steel ball zapper.

The first test with the new thruster was AS-56. Test point 56-1 was taken at the beginning of the test and shows good performance (Table 3). The total flow rate was only 1.87 times the desired one. At the end of 4 hours, glow spray began and the test was terminated. Visual examination of the rim showed no erosion; however, the thruster was warm. Figure 57 is the TOF trace of AS-56-1. One observation made during the glow-spray operation was the side beam divergence angle ($\approx 90^\circ$), which explains the high ratio of I_S/I_O .

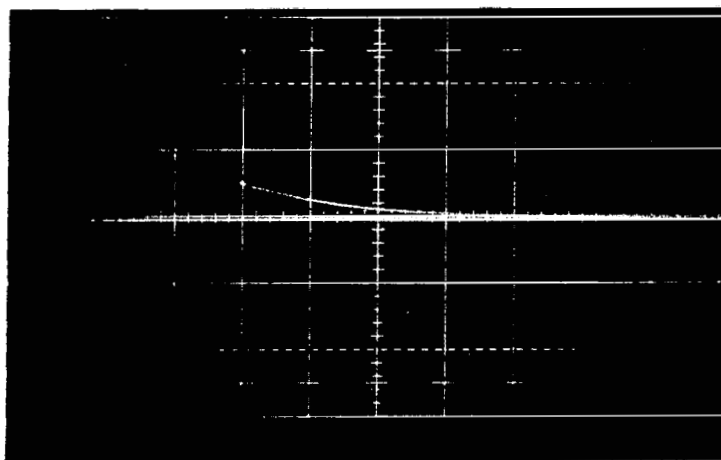


Figure 57—TOF trace of AS-56-1. $V_S = 19$ kV, $I_S = 60$ μ A, $i = 1$ μ A/cm, and the sweep was 10 μ sec/cm.

AS-57 was conducted using a positive extractor plate about one-fourth of an inch in front of the negative extractor plate. The attempt here was to provide a means by which the beam could be focused, which would reduce the beam divergence angle. The attempt was unsuccessful, and the positive plate was removed for the succeeding tests. The TOF is shown in Figure 58.

AS-58 was conducted using the NaI-1, 2, 6-hexanetriol solution (propellant No. 16). Four test points were taken during the test, which was terminated after approximately 3 hours of operation because of glow spray. This test very aptly demonstrates the degradation of performance due to propellant flow rate increase. Again, as in previous tests, there is strong indication that the propellant's temperature was raised by electron back bombardment. As the assumed electron back bombardment continued, the flow rate increased with a resultant decrease in performance. Finally the flow rate and vapor pressure reached a point at which glow spray commenced. This progression is reflected in test points 58-1 through 58-4.

It is interesting that the ratio I_S/I_O decreased from 18.7 for AS-56-1 to 7.35 for AS-58-1, which was run at a V_S of 3.5 kV lower than that for AS-56-1. The TOF traces for AS-58 are shown in Figures 13, 59, 60, and 61.

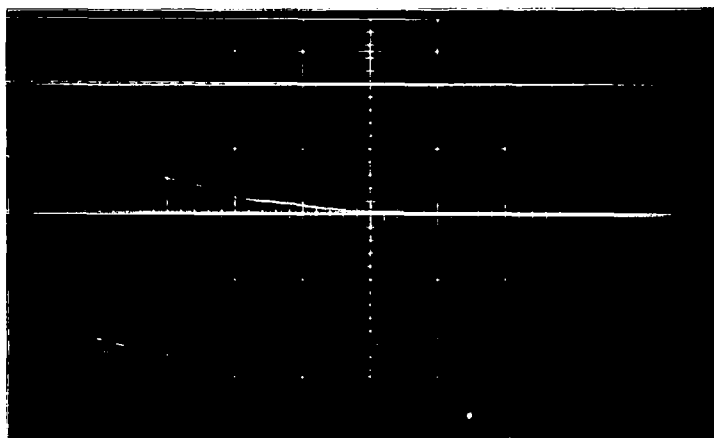


Figure 58—TOF trace of AS-57-2. $V_s = 19$ kV, $I_s = 45$ μ A, $i = 1$ μ A/cm, and the sweep was 50 μ sec/cm.

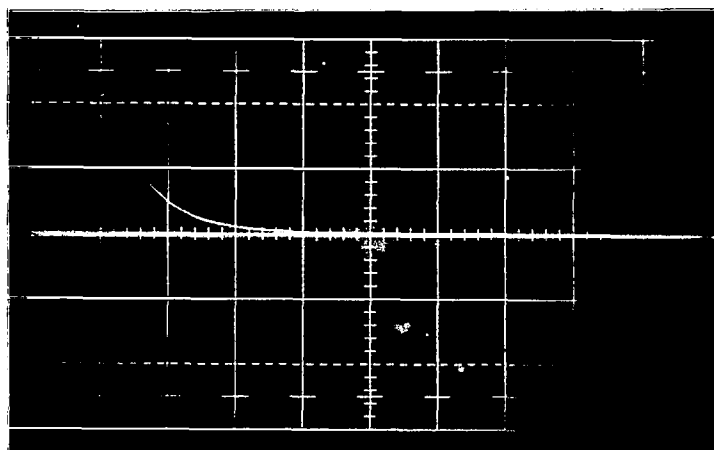


Figure 59—TOF trace of AS-58-1. $V_s = 15.5$ kV, $I_s = 50$ μ A, $i = 2$ μ A/cm, and the sweep was 20 μ sec/cm.

Unlike the results of glow spray on performance in previous NaI-glycerol tests (AS-35-9 through 35-21), where q/m and I_{sp} increased, it is seen here that q/m and I_{sp} decreased with increased glow spray. A possible explanation is that in tests AS-35-9 to 35-21 as the glycerol became hot, its vapor pressure became sufficiently high to evaporate before it was sprayed from the rims. Thus the vapor pressure was not reflected in I_C and, consequently, \dot{m}_C . However, as the 1,2,6-hexanetriol became hot, the predominant change was reflected in increased flow rate rather than increased evaporation. Therefore I_C increased, which reflected an increase in \dot{m}_C . This effect is shown in Table 3. Figures 60 and 61 also show a pronounced increase in slow particles at the tail end of the TOF traces reflecting lower q/m 's and higher \dot{m}_C .

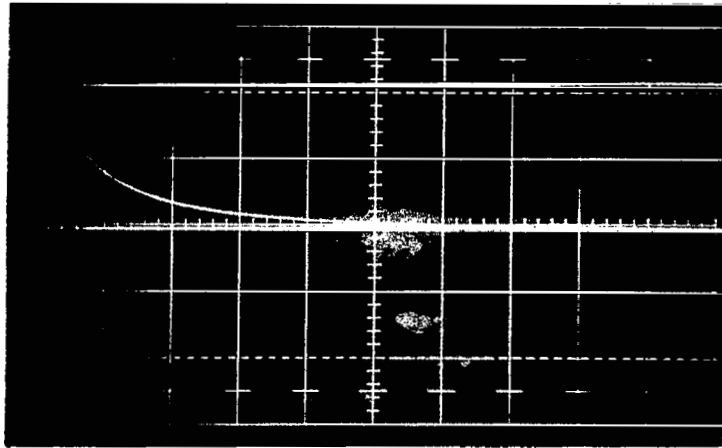


Figure 60—TOF trace of AS-58-3. $V_s = 16$ kV, $I_s = 270$ μ A, $i = 10$ μ A/cm, and the sweep was 20 μ sec/cm.

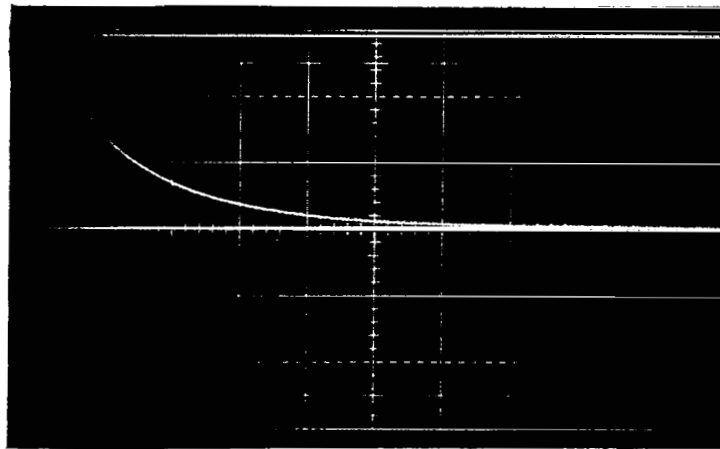


Figure 61—TOF trace of AS-58-4. $V_s = 17$ kV, $I_s = 350$ μ A, $i = 10$ μ A/cm, and the sweep was 20 μ sec/cm.

Examination after the test showed the thruster body to be at room temperature, which is reasonable considering the large thermal mass of this thruster. However, localized heating of the meniscus is possible without its being substantially reflected in the thruster mass.

This test closely ties together propellant heating, increased flow rate, and the resulting decrease in performance. Whether the results of glow spray in this test or those of test AS-35 are examined, the key factor that needs rigid control seems to be propellant heating, and at this time the most apparent cause for the heating is electron back bombardment.

CONCLUSIONS

The major effort of this program was concerned with obtaining acceptable thruster performance without the visible observance of glow spray at the thruster rims.

Efforts to accomplish this by minimization of exposed propellant surface area, variation of rim radii (changing of local field intensity), and elimination of feedline temperature rise (AS-37 through AS-43) were largely unsuccessful.

The attempts to achieve this through the reduction of propellant evaporation by the use of low-vapor-pressure solvents (AS-45 through AS-53) were, except for one propellant combination, generally unsuccessful. This one exception (AS-53-5) was accomplished with the lowest flow rate among the non-glow-spray tests. It was the first indication of a link connecting performance and glow spray.

Tests conducted with the standard NaI-glycerol solutions and using flow control orifices to duplicate the low flow rate achieved in AS-53-5 were unsuccessful because of the inability to control localized propellant heating and resulting glow spray, apparently caused by the back bombardment of the rims by electrons. The viscosity of 1,2,6-hexanetriol is more stable than that of glycerol during variations in temperature, which may be the reason why the low flow rates were maintained in AS-53-5.

Tests with the larger annular thruster using glycerol and 1,2,6-hexanetriol solvents doped with sodium iodide confirmed the previous indications that a flow rate much lower than the design value (Table 1) is required to achieve the performance goals of q/m and I_{sp} presented in Table 2. As a result of this necessarily low flow rate, a reduction in thrust is suffered. This is not detrimental, however, because the thrust level can be raised by the use of a multiple arrangement of thrusters.

One remaining problem is the glow spray that occurred after the successful performance of both the small and large thrusters (AS-53 and AS-58). It appears that if the non-glow-spray performance is sustained at a high q/m value for a given duration, glow spray eventually commences. A possible explanation for this is that the high-energy particles release secondary electrons from various impacted surfaces that find their way back to the exposed rim and propellant surfaces, which results in heating and causes increased propellant evaporation, flow rate, and propellant conductivity.

Based on the results of this program, to obtain the desired performance goals of q/m and I_{sp} under non-glow-spray conditions, the following suggestions seem to be promising means of solving the problem:

- (1) Use of sodium iodide and 1,2,6-hexanetriol as the propellant.
- (2) Reduction of flow rates until the desired q/m and I_{sp} are obtained and compensation for the thrust reduction by means of multiple thrusters.
- (3) Use of a center negative extractor (Reference 7) to reduce the heating effect caused by electron back bombardment.

ACKNOWLEDGMENTS

The authors wish to express their appreciation to Mr. Thomas Dennis who was responsible for the computer reduction of data during this program, to Dr. Allan Sherman for his contributions at the beginning of this program, and to Mr. Fred Gross and Dr. Ben Seidenberg for their advice and recommendations in our propellant investigations.

Goddard Space Flight Center
National Aeronautics and Space Administration
Greenbelt, Maryland, March 11, 1970
120-26-17-01-51

REFERENCES

1. Stark, K. W., "Design and Development of an Annular Slit Colloid Thruster," American Institute of Aeronautics and Astronautics Paper No. 69-287, American Institute of Aeronautics and Astronautics, 1290 Avenue of the Americas, New York, 1969.
2. Stark, K. W., and Sherman, A., "Research and Development in Needle and Slit Colloid Thrusters," NASA Technical Note D-5305, National Aeronautics and Space Administration, Washington, D.C., 1970.
3. Streeter, Victor L., "Fluid Mechanics," 4th ed., New York: McGraw-Hill Book Co., Inc., 1966.
4. Fuller, Dudley D., "Theory and Practice of Lubrication for Engineers," New York: John Wiley & Sons, Inc., 1956.
5. Cohen, E., "Research on Charged Colloid Generation," Air Force Aero Propulsion Laboratory Technical Document Report No. APL TDR 64-75, Air Force Aero Propulsion Laboratory, Research and Technology Division, Air Force Systems Command, Wright-Patterson Air Force Base, Ohio, June 1964.
6. Cohen, E., "Experimental Research to Determine the Feasibility of a Colloid Thruster," Air Force Aero Propulsion Laboratory Technical Report AFAPL-TR-65-72, Air Force Aero Propulsion Laboratory, Research and Technology Division, Air Force Systems Command, Wright-Patterson Air Force Base, Ohio, 1965.
7. "Colloid Thruster Technology," first and second quarterly reports for 1969-1970, NASA Contractor Reports 108177 and 108801, National Aeronautics and Space Administration, Washington, D.C., 1970.

NATIONAL AERONAUTICS AND SPACE ADMINISTRATION

WASHINGTON, D. C. 20546

OFFICIAL BUSINESS
PENALTY FOR PRIVATE USE \$300

FIRST CLASS MAIL



POSTAGE AND FEES PAID
NATIONAL AERONAUTICS AND
SPACE ADMINISTRATION

04U 001 53 51 3DS 71.10 00903
AIR FORCE WEAPONS LABORATORY /WLCL/
KIRTLAND AFB, NEW MEXICO 87117

ATT E. LOU BOWMAN, CHIEF, TECH. LIBRARY

POSTMASTER: If Undeliverable (Section 158
Postal Manual) Do Not Return

"The aeronautical and space activities of the United States shall be conducted so as to contribute . . . to the expansion of human knowledge of phenomena in the atmosphere and space. The Administration shall provide for the widest practicable and appropriate dissemination of information concerning its activities and the results thereof."

— NATIONAL AERONAUTICS AND SPACE ACT OF 1958

NASA SCIENTIFIC AND TECHNICAL PUBLICATIONS

TECHNICAL REPORTS: Scientific and technical information considered important, complete, and a lasting contribution to existing knowledge.

TECHNICAL NOTES: Information less broad in scope but nevertheless of importance as a contribution to existing knowledge.

TECHNICAL MEMORANDUMS: Information receiving limited distribution because of preliminary data, security classification, or other reasons.

CONTRACTOR REPORTS: Scientific and technical information generated under a NASA contract or grant and considered an important contribution to existing knowledge.

TECHNICAL TRANSLATIONS: Information published in a foreign language considered to merit NASA distribution in English.

SPECIAL PUBLICATIONS: Information derived from or of value to NASA activities. Publications include conference proceedings, monographs, data compilations, handbooks, sourcebooks, and special bibliographies.

TECHNOLOGY UTILIZATION PUBLICATIONS: Information on technology used by NASA that may be of particular interest in commercial and other non-aerospace applications. Publications include Tech Briefs, Technology Utilization Reports and Technology Surveys.

Details on the availability of these publications may be obtained from:

SCIENTIFIC AND TECHNICAL INFORMATION OFFICE

NATIONAL AERONAUTICS AND SPACE ADMINISTRATION

Washington, D.C. 20546